

**TAMPERE UNIVERSITY OF
TECHNOLOGY
ELECTRONICS LABORATORY**

Tutkimusraportti n:o 2/1984

Research Report No. 2/1984

OPTIMIZATION OF SQUID VECTOR GRADIO-
METER

J.O. Lekkala and J.A.V. Malmivuo

**TAMPEREEN TEKNILLINEN KORKEAKOULU
ELEKTRONIIKAN LABORATORIO**

**P.O.B. 527 SF-33101 TAMPERE 10
FINLAND**



Tutkimusraportti n:o 2/1984
Research Report No. 2/1984

OPTIMIZATION OF SQUID VECTOR GRADIOMETER

J.O. Leikkala and J.A.V. Malmivuo

15.6.1984

ISBN 951-720-871-5

OPTIMIZATION OF SQUID VECTOR GRADIOMETER

J.O. Lekkala and J.A.V. Malmivuo

ABSTRACT

We have optimized the structure and dimensions of a vector gradiometer designed for magnetocardiographic studies with the unipositional lead system. The optimization was made with respect to the signal-to-noise ratio for a limited space in cryostat, when the gradiometers were coupled to thin-film SQUIDs. The accuracy of determining the magnetic dipole source from the measured magnetic coil flux was examined with different circular and rectangular coils in coaxial and planar gradiometers. The effective flux-transfer factor which takes into account the interdependence of the flux noise and SQUID's inductance was derived. In all cases three different basic gradiometer structures were optimized, one symmetric and two asymmetric gradiometers where the ratio between the areas of the second and pick-up coil was 2 and 3. It was found that the optimum structure depends on the cryostat's inner radius. The best accuracy is obtained by using a circular coil with an appropriate length which depends on the turn density of the coil.

CONTENTS

1. INTRODUCTION	1
1.1. Vector magnetocardiography	1
1.2. Detection coil	2
2. GRADIOMETER DIMENSIONS	4
2.1. Coil dimensions	4
2.1.1. X coil	5
2.1.2. Y coil	8
2.2. Baseline	9
2.2.1. Proximity effect	13
3. INDUCTANCE OF THE GRADIOMETER	15
4. FLUX-TRANSFORMER	17
4.1. Thin-film SQUIDS	17
4.2. Coupling of the detection coil to the SQUID	18
4.3. Signal-to-noise ratio	19
4.4. Effect of SQUID's inductance on the noise	21
5. OPTIMIZATION EQUATIONS	25
5.1. Source models	25
5.2. Signal-to-noise ratio	26
5.3. Sensitivity	29
6. RESULTS	30
6.1. X gradiometer	30
6.1.1. Effect of the pick-up coil length	30
6.1.2. Effect of the Y coil radius	36
6.1.3. Effect of the source type	37
6.2. Y and Z gradiometer	39
6.2.1. Circular coils	39
6.2.2. Rectangular coils	40
6.3. Optimum construction of vector gradiometer	41
7. DISCUSSION	44
8. SUMMARY	47
REFERENCES	49

1. INTRODUCTION

1.1. Vector magnetocardiography.

The aim of magnetocardiography (MCG) is to determine the clinical condition of the heart muscle from the measured magnetic field data. There does not exist any unique solution for this *inverse problem*. The heart contains no magnetic material, but the magnetic field is generated by a distributed electric current density $\vec{J}(\vec{r})$ in the heart muscle. However, by using simplified models for the source distribution and the volume conductor, the parameters of the *equivalent generator* can be solved. The equivalent magnetic dipole source of MCG is called the *magnetic heart vector* (MHV) and it describes the magnetic field of all elementary dipoles. The sensitivity of a detector coil to the position and orientation of the source current density can be analyzed by *lead field theory*.

There exist three different lead systems for determining the magnetic heart vector: the XYZ-lead presented first by Baule and McFee [Bau 70], and the ABC-lead and unipositional lead introduced by Malmivuo [Mal 78]. According to the studies of Malmivuo, the best lead system for recording the MHV is the unipositional lead system. In this system the detector is positioned at a single point on the anterior side of the chest so that all three components of the MHV can be recorded by simply changing the detector's orientation, not its position. By using a three channel instrument the MHV can be recorded in real time. One way to orientate the coils is presented in Fig. 1. Theoretically the magnetic heart vector (\vec{m}) components can be obtained from the components of the magnetic field vector \vec{B} by the following matrix operation:

$$\begin{pmatrix} m_x \\ m_y \\ m_z \end{pmatrix} = \frac{2\pi r^3}{\mu_0} \begin{pmatrix} 1 & 0 & 0 \\ 0 & -2 & 0 \\ 0 & 0 & -2 \end{pmatrix} \begin{pmatrix} B_x \\ B_y \\ B_z \end{pmatrix}, \quad (1)$$

where r = the distance between the source dipole and the measurement point.

Eskola *et al.* have tested the ideality and sensitivity of several vector magnetocardiographic leads by using an inhomogeneous, physical torso

model [Esk 84]. They have found that the so called corrected unipositional lead system best fulfills the clinical requirements. In this system the field vector is measured on the anterior chest 15 mm in the cranial direction from the center of the heart. The magnetic heart vector is obtained from the field vector by using Eq. (1), but now with the multiplication term -1 for Y and Z components instead of -2 .

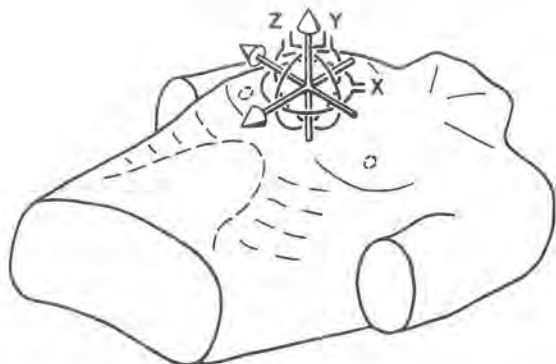


Figure 1. Location of the detection coils in the unipositional lead system.

1.2. Detection coil

At present biomagnetic measurements are made with SQUID magnetometers where a gradiometer type detection coil construction is normally used [Coh 70, Zim 71]. The construction and dimensions of the detection coil determine what are the signal-to-noise ratio and the sensitivity and accuracy of the measurement. The maximum available signal-to-noise ratio depends on the matching of the inductances between the detection coil and SQUID's signal coil. Also the structure of the SQUID has an effect on its own intrinsic noise level, self-inductance and the coupling coefficient between the signal coil and the SQUID ring. There have been presented several types of gradiometers in the literature. They are normally designed according to the maximum flux-transfer [Cla 75], maximum sensitivity [Zim 77], or other detailed requirements as for example

the directivity [Kar 80], finding the direction of current sources [Coh 82], or insensitivity to a given type of noise [Vrb 82, Bru 83, Sto 83]. The effect of the dimensions of the gradiometer has been studied with respect to the matching [Ode 78], but also with respect to the field source [Wik 78, Wil 81, Rom 82]. Duret and Karp [Dur 83] have presented for the flux-transformer a figure of merit which takes into account the flux-transformer parameters and the nature of the source. The only superconducting vector gradiometer designs have been presented by authors [Lek 82, Lek 84] and Varpula *et al.* [Var 82, Sep 83]. All studies are normally made without taking into consideration the limiting space of the cryostat where the gradiometer is used.

When the gradiometer is optimized for an unlimited space, the result is usually different from that when it is optimized for a given dimension of the inner Dewar in such a way that the distance from the tip of the Dewar to the source is fixed (minimum measurement distance). The accuracy of the measurement depends on the ratio between the dimensions of the pick-up coil and the distance to the source. Also the baseline i.e. the distance between the gradiometer coils is important. The accuracy in this case means the same as the spatial resolution. If the spatial resolution is poor, the result when determining the source from the measured flux is not correct. Thus the detector coil should be designed according to the source's type.

The purpose of this study was to find a vector gradiometer structure which would give the maximum sensitivity together with minimum error when determining the MHV. The optimization was made with respect to the signal-to-noise ratio because this is the most important factor affecting the quality of the measurement. A further aim was to examine the effect of the gradiometer baseline on the S/N-ratio and of the gradiometer coil dimensions on the accuracy of the measurement.

2. GRADIOMETER DIMENSIONS

An example of the geometry of a real vector gradiometer is shown in Fig. 2. This vector gradiometer coil system consists of three first-order gradiometers wound on a common core with thin niobium wire. The X gradiometer which measures the field gradient perpendicular to the patient's chest (dB_x/dx) is constructed coaxially. In the Y and Z directions there are coplanar gradiometers which measure the off-diagonal component of the magnetic field gradient ($dB_y/dx, dB_z/dx$). All gradiometers are designed so that their sensitivities, i.e. areas and number of turns, are equal.

The gradiometers which were examined in this study are all first-order constructions. The circular cross-section was chosen for the X gradiometer's coils. In the Y and Z gradiometers both coils with circular and rectangular cross-sections were studied. We next examine the effect of the gradiometer dimensions on the measurement result. This study is made assuming the source to be a magnetic dipole.

2.1. Coil dimensions

Because the SQUID measures the magnetic flux Φ_d of the detector coil, the magnetic flux density \bar{B} at the measurement point must be calculated by using the effective area and number of turns of the coil. If the coil consists of N_d loops, the axial component of the magnetic flux density in the center of the coil can be calculated as

$$\bar{B} = \frac{\Phi_d}{N_d A_e} \bar{n} \quad , \quad (2)$$

where A_e = the effective area of the coil,
 \bar{n} = the unit vector along the coil axis.

If the coil is large, the flux is not constant inside it and the calculated flux density is not necessarily equal to the true axial component of the flux density in the center of the coil. Consequently the coil should be as small as possible for accurate results when recording magnetic fields with high spatial gradients or field pattern having fine details. However, a compromise must be made between sensitivity and spatial resolution.

2.1.1. X coil

Let a coil with the radius R and number of turns N_d be on the positive X axis at the distance h from the origin to its center so that its axis coincides with the X axis (Fig. 3a). Then the magnetic coil flux generated by a magnetic dipole \bar{m} which is in the origin and oriented along the X axis can be expressed as

$$\Phi_d = \frac{\mu_o m}{2} \sum_{i=1}^{N_d} \frac{R^2}{(R^2 + h_i^2)^{3/2}}, \quad (3)$$

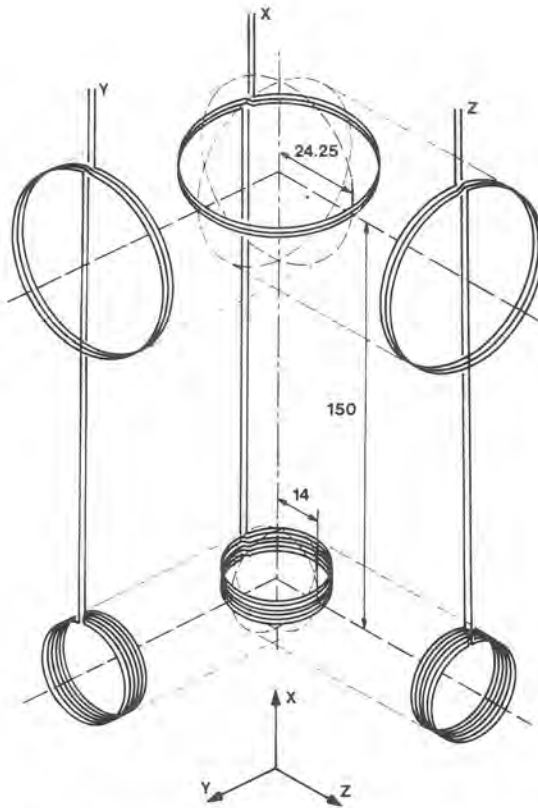


Figure 2. Coil construction of an asymmetric vector gradiometer. For clarity, different gradiometers are drawn apart. Dimensions are given in millimetres.

where h_i is the distance between the dipole and the i :th loop of the coil. Here and in the following analysis we have assumed that each loop of the coil is on a plane perpendicular to the coil axis and that the distance between the planes is equal to $l/(N_d - 1)$, where l is the length of the coil. By inserting the flux calculated from Eq. (3) to Eq. (2) we get an approximation for the axial component of the magnetic flux density in the coil center. In Fig. 3a the ratio between two flux densities B_{ave} and B_{dip} , generated by a magnetic dipole is shown as a function of R/h with different ratios of l/R . B_{ave} is the average flux density inside the coil calculated from the coil flux by using Eq. (2) and Eq. (3). B_{dip} is the axial magnetic flux density in the center of the coil calculated from the dipole equation

$$B_{dip} = \frac{\mu_0 m}{2\pi h^3} \quad (4)$$

The best accuracy is obtained when the ratio l/R is of the order of 1.73 (Fig. 3a). With this kind of coil the distance h can be equal to $3R$ and still the error is below 1% when determining the magnetic flux density in the center of the coil from the measured coil flux. If l/R differs much from 1.73, the distance h must be longer for the same maximum error. In the designing of the coil the shortest possible measurement distance for a given maximum error is obtained if a small error in the positive direction is allowed. When $l/R > 1.73$ the result is greater or the error is positive when l is long. When the source is very close to the coil the error will be negative. When $l/R < 1.73$ the error is always negative. In the case $l/R = 0$ there is only one turn of infinite thin wire. The exact value for optimum l/R -ratio is obtained if the field generated by the current in a solenoid is expressed in a Taylor series expansion. When the ratio of the length and radius of the solenoid are related as $l/R = \sqrt{3}$ the field contains a dipole moment but no quadrupole moment. Octapole and higher moments are present but contribute less than 1% of the field at the distance $4R$ from the coil [Wik 75].

However, the optimum value for l/R is $\sqrt{3}$ when the turns of the coil are closely wound. If the turn density is smaller, then the optimum value of l/R tends to decrease. The limiting case is when there are only two loops so that the pitch is equal to the length of the coil. Then the optimum value of l/R is 1. This result is in good agreement with the Helmholtz array, which is a pair of identical circular loops separated by the radius of the loop and has a vanishing third-order moment [Sto 83].

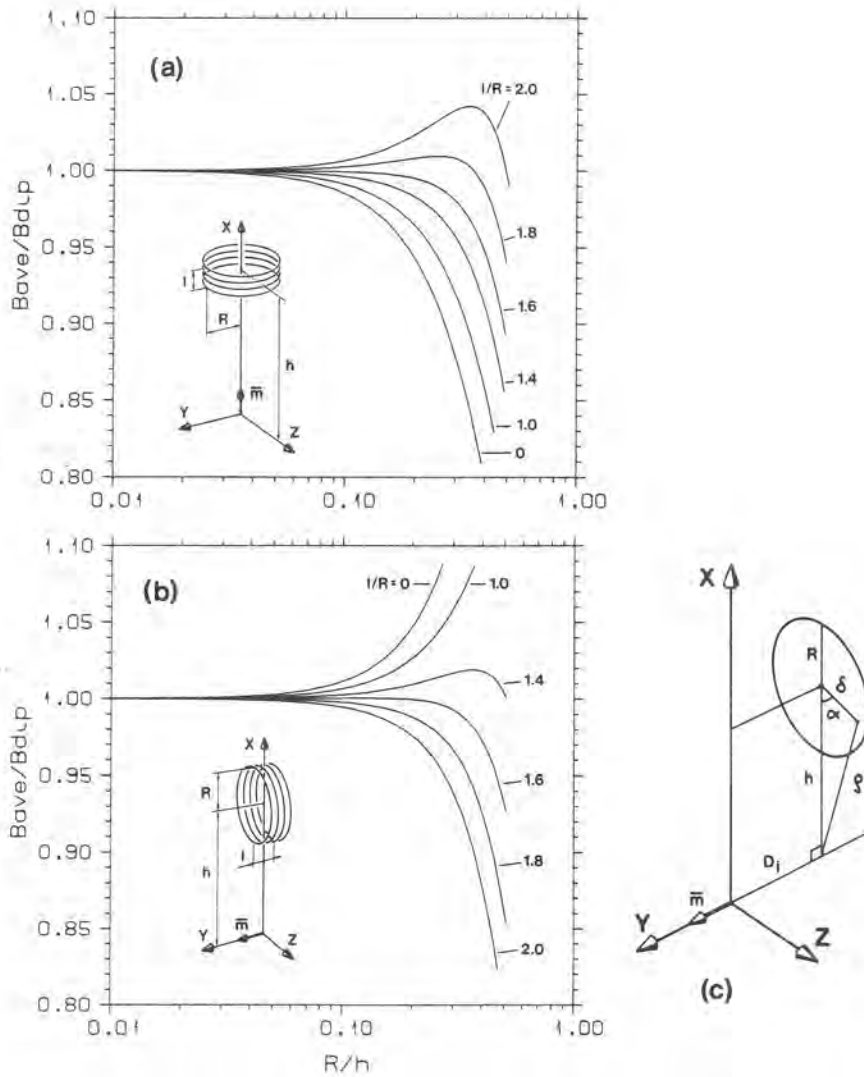


Figure 3. Ratio of the magnetic flux density B_{ave} , calculated from the coil flux, to the flux density B_{dip} , calculated from the dipole equation, in the center of the coil with different ratios of l/R . (a) The source is a magnetic dipole \bar{m} located coaxially with the coil; (b) the magnetic dipole source and the coil center are located on the same plane which is perpendicular to the coil axis. In both cases the coils are circular and the turn density of the coils is $10/R$; (c) parameters of Eqs. (5) and (30) when calculating the flux through the circular Y loop.

2.1.2. Y coil

Circular coil

Let us have a similar case as above but now so that the coil axis is directed along the Y axis and the magnetic source dipole \vec{m} in the origin is directed in the same direction (Fig. 3b). In this case of Y coil (situation with Z coil is equal) we can calculate the magnetic flux of the coil according to the following equation:

$$\Phi_d = -\frac{\mu_o m}{4\pi} \sum_{i=1}^{N_d} \int_0^{2\pi} \int_0^R \frac{2D_i^2 - \rho^2}{(\rho^2 + D_i^2)^{5/2}} \delta d\delta d\alpha \quad (5)$$

where $\rho^2 = h^2 - 2h\delta \cos \alpha + \delta^2$

The parameters of this equation are shown in Fig. 3c. The double integral of Eq. (5) has been computed numerically. In Fig. 3b the relative flux density B_{ave}/B_{dip} is shown as a function of R/h for different ratios of l/R . B_{dip} is again the magnetic flux density in the center of the coil and now calculated according to the dipole equation from

$$B_{dip} = \frac{\mu_o m}{4\pi h^3} \quad (6)$$

When the turn density of the coil is high, the optimum l/R -ratio is about 1.5. In the Y coil the optimum ratio differs from that value of $\sqrt{3}$ obtained from the Taylor series expansion. This is possibly caused by the fact that the source is not on the coil axis. Now the change in the l/R -ratio produces an effect opposite to that produced in the case of the X coil. When l/R is greater than 1.5, the B_{ave}/B_{dip} -ratio is below one or the error is negative, and when $l/R < 1.5$, the error is first positive and after that negative if the R/h is further increased. Again, if a coil with only two turns is analyzed, the optimum value of l/R seems to be about 0.9.

As can be seen from the discussion above, the detector coil with circular cross-section should be designed carefully if the measurement is made closer than $10R$ from the source. Thus the pick-up coil's length-to-radius ratio should be between 0.9-1.73 depending on the value of the coil's turn density. When the distance to the source is longer than $10R$, the dimensions of the coil are not very critical.

Rectangular coil

The effect of the coil dimensions on the measurement accuracy was examined also with rectangular coils. When the coil and the source dipole are directed as shown in Fig. 4a, the magnetic flux of the coil is

$$\Phi_d = \frac{\mu_0 m_y}{2\pi} \sum_{i=1}^{N_1} \int_0^{C/2} \int_{-A/2}^{A/2} \frac{2D_i^2 - \rho^2}{(\rho^2 + D_i^2)^{5/2}} dx' dz' \quad (7)$$

where $\rho_1^2 = (h + x')^2 + z'^2$.

The parameters of this equation are shown in Fig. 4d. The double integral has again been calculated numerically. The relative flux density B_{ave}/B_{dip} is shown as a function of $(A/2)/h$ for different ratios of $l/(C/2)$ in three cases, where the cross-section area of the coil is a square (Fig. 4a), one half of the square (Fig. 4b) and one third of that (Fig. 4c). In all cases the width C of the coil is the same, but in Figs. 4b and 4c the height A is one half and one third of that in Fig. 4a, respectively. The flux density B_{dip} is calculated from Eq. (6). With rectangular coils longer measurement distances are needed for equal accuracy with the circular coils. It is possible to measure with an error of less than 3% only at distances greater than 15C-20C.

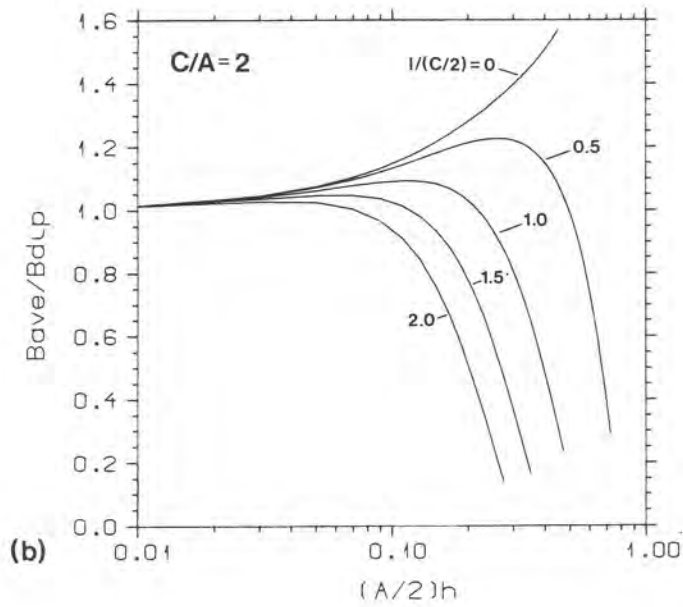
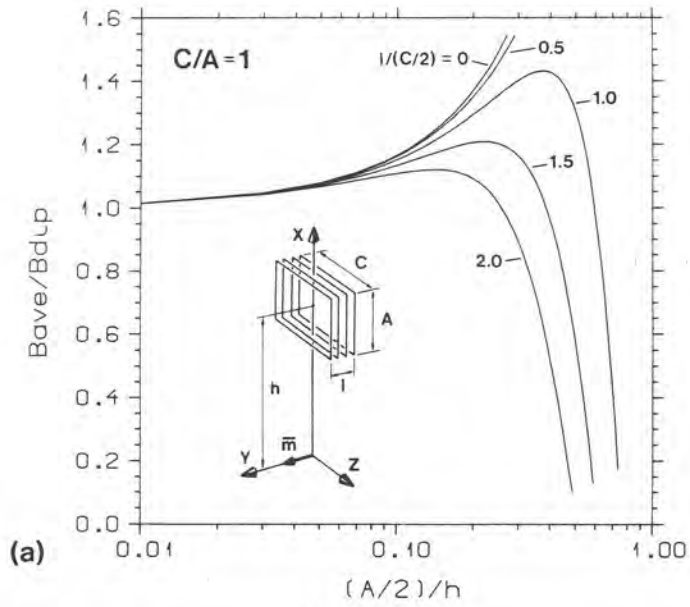
2.2. Baseline

For biomagnetic measurements the gradiometer baseline is large when compared to the distance from the gradiometer to the signal source and small when compared to the distance from the noise sources. The magnetic field difference which is detected by a first order gradiometer from a magnetic dipole source can be written as [Vrb 82]

$$\Delta B_1 = \frac{cm}{r^3} - \frac{cm}{(r+b)^3} = B_0 \left(1 - \frac{1}{(1+\alpha)^3} \right) \quad (8)$$

where $c = \text{constant}$,
 $m = \text{the magnetic dipole moment of the source}$,
 $r = \text{the distance from the source to the field point}$,
 $b = \text{the baseline}$,
 $\alpha = b/r$.

When a dipole source is near to the pickup coil of the gradiometer or when $\alpha \gg 1$ in Eq. (8), the gradiometer behaves as a magnetometer or



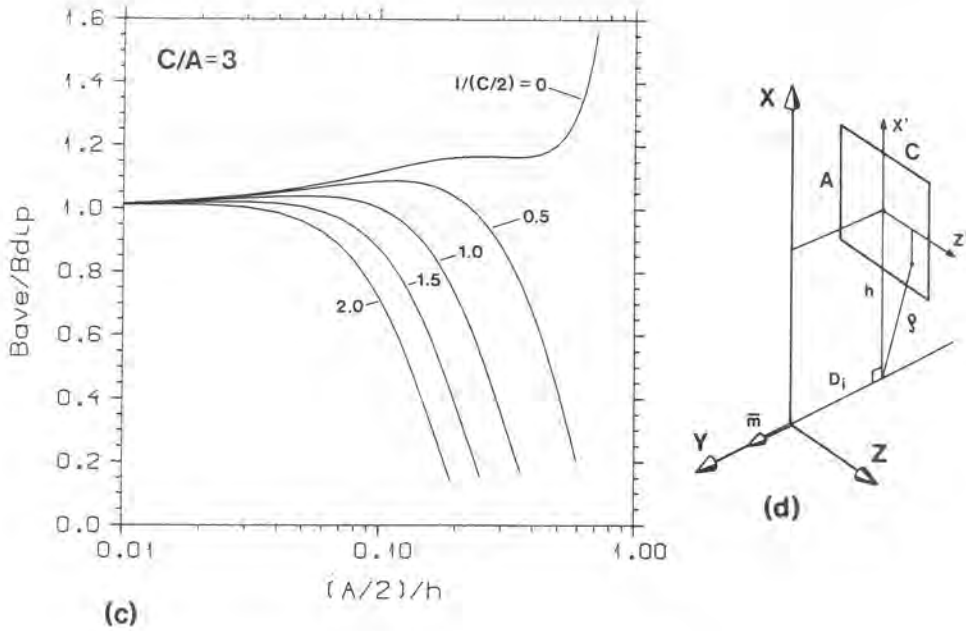


Figure 4. Ratio of the magnetic flux density B_{ave} , calculated from the coil flux, to the flux density B_{dip} , calculated from the dipole equation, in the center of a rectangular coil with different ratios of $l/(C/2)$. The magnetic dipole source and the coil center are located on the same plane which is perpendicular to the coil axis; (a) the cross-section area of the coil is a square; (b) the height of the coil is one half of that of the square coil; (c) the height of the coil is one third of that of the square coil. In all cases the width C of the coil is constant and the turn density of the coils is $20/C$; (d) parameters of Eqs. (7) and (31) when calculating the flux through the rectangular Y loop.

$\Delta B_1 \approx B_o$. For distant interference sources this differential magnetometer responds as a true gradiometer. Generally, in biomagnetic measurements it is more useful to measure the field rather than its gradient and so the baseline of a differential magnetometer should be somewhat longer than the characteristic dimension of the source [Wik 78]. The heart can be modelled with a sphere whose radius is 56 mm [Mal 76]. The center of the heart is located about 70 mm from the outer surface of the anterior chest, Fig. 5. On account of this the baseline should be greater than 112 mm.

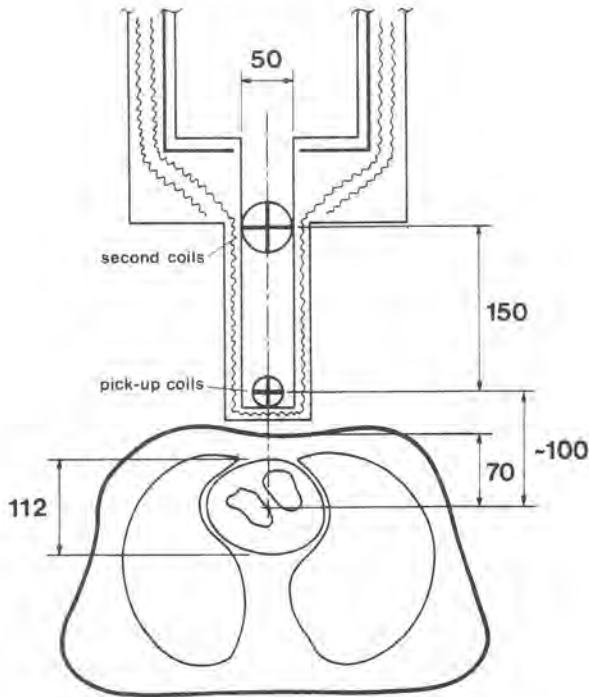


Figure 5. Location of the vector gradiometer during the unipositional measurement. The vector gradiometer is inside a Dewar which is above the heart as close to the anterior chest as possible. Dimensions given in mm.

2.2.1. Proximity effect

The sensitivity of the detector coil varies according to the source location in the heart. The fact that the coil is more sensitive to the sources in the anterior heart muscle than in the posterior region is known as *proximity effect*. In the unipositional lead this proximity effect is the main reason for the inhomogeneity of the lead [Mal 76, Esk 83]. If the baseline is shortened in the gradiometer, the proximity effect will be increased.

Although a ball with a radius of 50 mm is a good approximation for the physical heart, it is obvious that when modelling the mean electrical activity with respect to the thickness of the myocardium a somewhat smaller radius can be used [Esk 83]. The radius of the "active" heart is in the following analysis estimated to be 50 mm. In Fig. 6 the effect of the baseline is shown. The ratio of the anterior and posterior sensitivity of a gradiometer compared to that of a magnetometer is plotted as a

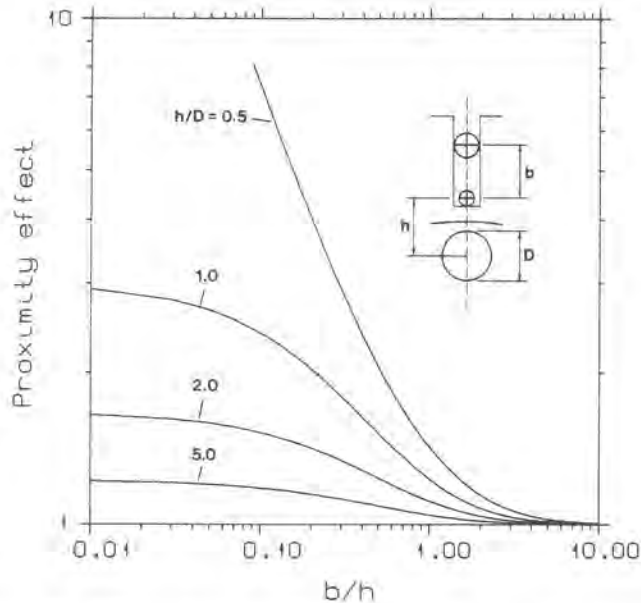


Figure 6. Effect of the gradiometer baseline on the proximity effect. The ratio of anterior and posterior sensitivities for an ideal gradiometer compared to that of a magnetometer is plotted as a function of the baseline/distance-ratio in four cases, when the ratio between the distance h from the center of the pick-up coil to the source and the diameter D of the source volume is $h/D = 0.5, 1, 2$ and 5 .

function of the baseline/distance ratio. The ratio between gradiometer and magnetometer is calculated in four cases, when the distance between the pick-up coil and center of heart is 0.5, 1, 2 and 5 times the diameter of the heart model. The same curves describe the effect of the baseline in both X and Y directions. The curves of Fig. 6 are calculated by using Eq. (8) when the distance from the center of the heart is equal to 100 mm (Fig. 5). The minimum anterior and maximum posterior measurement distances are thus 50 mm and 150 mm, respectively.

Shortening the baseline will improve the signal-to-noise ratio only until the baseline is somewhat shorter than the distance to the source. After that the gradiometer acts as a true gradiometer for both the distant noise sources and the nearby signal sources [Wik 78, Vrb 82]. According to the limits imposed above the baseline was chosen to be 150 mm long. Thus in this case, when $h = 100$ mm, the proximity effect is increased by only 12.5 %, and the signal from a dipole source (assumed to be in the center of the heart) is attenuated by the second coil by 6.4 % when compared to the magnetometer.

3. INDUCTANCE OF THE GRADIOMETER

The inductance of a single-layer solenoid in the situation where the coil length l is smaller than its radius R can be expressed by the approximative equation [Lan 67]

$$L_d = \mu_o N_d^2 R \left(\ln \frac{8R}{l} - \frac{1}{2} \right) = \lambda_d N_d^2 \quad ; l < R. \quad (9)$$

When the coil is long the inductance is given by [Gro 46]

$$L_d = \mu_o N_d^2 \frac{\pi R^2}{l} \left(\frac{1}{1 + 0.9R/l} \right) = \lambda_d N_d^2 \quad ; l > 0.8R. \quad (10)$$

The inductance of the coil depends in addition on the number of turns on the geometrical factor λ_d . In Fig. 7 the normalized inductance L_d is shown as a function of the ratio l/R calculated from Eqs. (9) and (10). For the optimization we have used both equations with the limit $l = 0.6R$. For a good signal-to-noise ratio λ_d should be as small as possible when the coil is coupled to a SQUID. Thus for a given coil area we can increase the number of turns when the coil is made longer while the inductance remains the same.

The inductance L_g of a first order gradiometer with the number of turns N_1 and N_2 in the pick-up coil and second coil, respectively, can be expressed as

$$L_g = L_1 + L_2 - 2 \sum_{i=1}^{N_1} \sum_{j=1}^{N_2} M_{ij} \quad , \quad (11)$$

where L_1 = the inductance of the pick-up coil,
 L_2 = the inductance of the second coil,
 M_{ij} = the mutual inductance between the i :th turn of the pick-up coil and the j :th turn of the second coil.

If the inductance of a symmetric gradiometer is calculated with the coil radius of 25 mm, coil length of 2 mm, number of turns 9 in both coils and baseline of 150 mm (dimensions typical for our case) we get by using Eq. (11) $L_g = 10.4 \mu H - 34 nH$ where the latter part is the mutual inductance of the two coils calculated according to Grover [Gro

46]. Because of the relatively large baseline the mutual inductance is insignificant when compared to the sum of the coil inductances. Because of its opposite sign it also compensates for the inductance of the connection wires which is of the same order. According to this result, and because the length of the baseline is fixed in our study, the effect of the mutual inductance between the coils is omitted in the following examination.

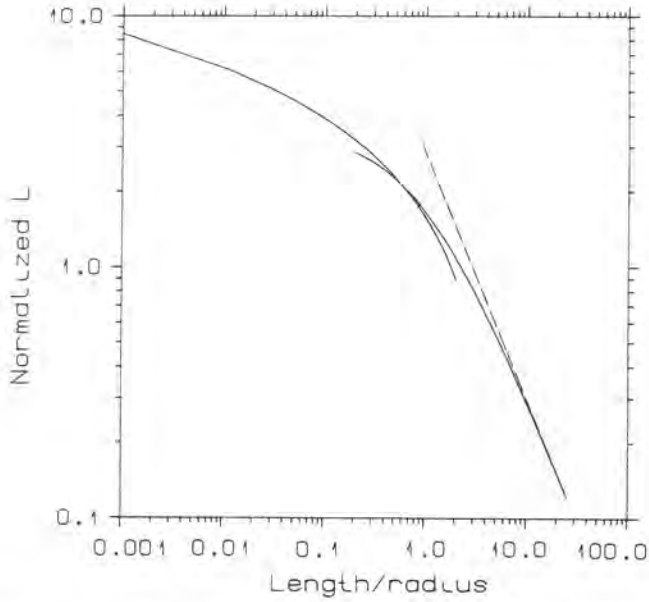


Figure 7. Normalized inductance $L_d(\mu_o N_d^2 R)^{-1}$ of a solenoid as a function of l/R calculated by using Eqs. (9) and (10). The dashed line corresponds to the formula $L_d = \mu_o N_d^2 \pi R^2 l^{-1}$.

4. FLUX-TRANSFORMER

The effective area of a SQUID is of the order of a few mm^2 in maximum. Because the sensitivity to the magnetic field is proportional to the detector's area, the "capture area" of the SQUID is normally increased in biomagnetic measurements by using a flux-transformer. This consists of a closed loop of superconducting wire formed by the signal coil and detection coil.

4.1. Thin-film SQUIDS

The RF-SQUIDS which we have used are thin-film SQUIDS formed by four loops in parallel across an Nb-Nb oxide-Pb tunnel junction. The devices have been designed and fabricated by Ehnholm *et al.* [Ehn 75]. The glass substrate with the thin-film structure is pressed against the top of a niobium ring block. The signal coil is wound on the block surface and the RF-coil is divided into the four holes of the block. The basic electric data and characteristics of this type of thin-film SQUID are presented in Table 1.

Table 1. Electric data of the thin-film SQUIDS

Self-inductance L , nH	0.25
Signal coil inductance L_s , μH	20
Tank coil inductance L_t , nH	160
Coupling coefficient k_s	0.3
Energy sensitivity E_i , $J(Hz)^{-1}$	$2.7 \cdot 10^{-27}$

4.2. Coupling of the detection coil to the SQUID

The coupling of the detection coil to the SQUID's signal coil and the corresponding equivalent circuit is presented in Fig. 8. The total magnetic flux through the superconducting flux transformer remains constant. The signal coil flux Φ_s can be written as [Lou 75]

$$\Phi_s = L_s i_s - M_s i_{sq} = L_s i_s - \frac{M_s^2 i_s}{L}, \quad (12)$$

where L = the self-inductance of the SQUID,
 L_s = the inductance of the signal coil of the SQUID,
 i_s = the current of the flux-transformer,
 i_{sq} = the current of the SQUID,
 M_s = the mutual inductance between the signal coil and the SQUID.

Equation (12) can be further written as

$$\Phi_s = L_s \left(1 - \frac{M_s^2}{L_s L}\right) i_s = L_s (1 - k_s^2) i_s = L_{eff} i_s, \quad (13)$$

where L_{eff} = the effective self-inductance of the signal coil,
 $k_s = M_s / \sqrt{L_s L}$ is the coupling coefficient between the signal coil and the SQUID.

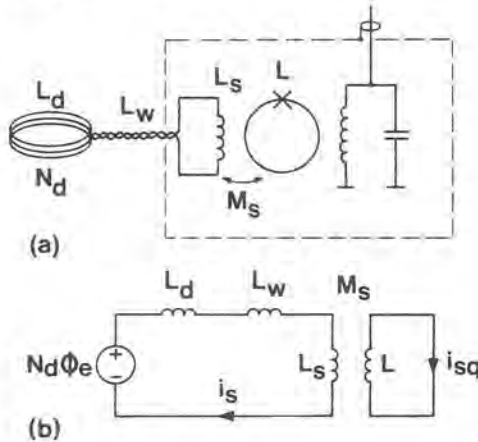


Figure 8. Coupling of the detection coil to the SQUID; (a) parameters of the coupling (broken line describes the superconducting shield); (b) equivalent circuit of the input coupling.

A change in the external flux $\Delta\Phi_e$ causes a change in i_s which induces a flux change $\Delta\Phi_{sq}$ in the flux going through the SQUID. The flux transfer factor F is the ratio between the SQUID flux and the external flux or

$$F = \frac{\Delta\Phi_{sq}}{\Delta\Phi_e} = \frac{N_d M_s}{L_d + L_{eff}} = \frac{N_d k_s (L_s L)^{1/2}}{L_d + (1 - k_s^2) L_s} \quad (14)$$

where N_d = the number of turns of the detection coil,
 L_d = the inductance of the detection coil

and where the signs of the fluxes are not taken into consideration. The inductance L_w of the pair of coupling leads which are tightly twisted together is of the order of $0.3 \mu H$ per meter [Lou 75]. It is small when compared to the value of L_s (Table 1) and can be neglected in this equation.

The optimum flux transfer condition is achieved when Eq. (14) is maximized. By taking the derivative with respect to L_s it can be seen that the maximum condition is obtained when

$$L_s = \frac{L_d}{(1 - k_s^2)} \quad (15)$$

Thus the inductance of the detector coil should be equal to the effective inductance of the signal coil, Eq. (13). This condition of matched inductances is analogous to the requirement that an amplifier's input impedance should be matched to the source impedance for maximum power gain [Cla 75]. The maximum value of the flux transfer factor of Eq. (14) is then

$$F_{max} = \frac{k_s N_d}{2(1 - k_s^2)^{1/2}} \left(\frac{L}{L_d} \right)^{1/2} \quad (16)$$

In Fig. 9 there are shown the normalized flux transfer factor as a function of the ratio between the signal coil and detection coil inductances L_s/L_d for different values of coupling coefficient k_s calculated for the thin-film SQUIDs used (Table 1). For high values of k_s the maximum occurs at relatively small values of L_d when compared to the L_s . For low values of k_s the matching of the detector coil to the signal coil seems to be more critical.

4.3. Signal-to-noise ratio

When a flux transformer is used the maximum flux sensitivity of the system is equal to the value of the flux in the detector coil which generates

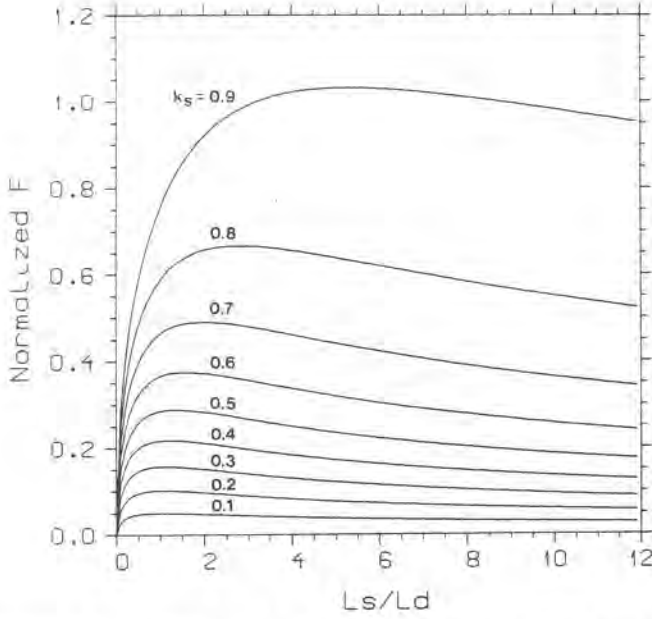


Figure 9. Normalized flux-transfer factor $F(L/L_d)^{-1/2}$ as a function of L_s/L_d for different values of the coupling coefficient k_s .

in the SQUID a flux equal to its intrinsic flux noise $\langle \Phi_{ni}^2 \rangle^{1/2}$. Next it is assumed that the flux noise is constant or does not depend on SQUID's self-inductance. In the optimum coupling condition it follows from Eq. (16) that the minimum detectable flux change through the detector coil is

$$\Delta \Phi_{min} = \frac{\langle \Phi_{ni}^2 \rangle^{1/2}}{F_{max}} = \frac{2(1 - k_s^2)^{1/2} \sqrt{L_d}}{N_d} \cdot \frac{\langle \Phi_{ni}^2 \rangle^{1/2}}{k_s \sqrt{L}} \quad (17)$$

By using Eq. (16) the maximum signal-to-noise ratio of the system can be determined as

$$\frac{S}{N} |_{max} = \frac{\Delta \Phi_{sq}}{\langle \Phi_{ni}^2 \rangle^{1/2}} = \frac{k_s N_d}{2(1 - k_s^2)^{1/2}} \cdot \left(\frac{L}{L_d} \right)^{1/2} \cdot \frac{\Delta \Phi_e}{\langle \Phi_{ni}^2 \rangle^{1/2}} \quad (18)$$

where $\Delta \Phi_{sq}$ is the flux change in the SQUID caused by the external flux change $\Delta \Phi_e$ in the detection coil. The maximum available S/N-ratio in a real measurement situation is obtained if the SQUID's intrinsic noise flux $\langle \Phi_{ni}^2 \rangle^{1/2}$ in Eq. (18) is replaced with the total equivalent noise flux $\langle \Phi_n^2 \rangle^{1/2}$ of the system.

4.4. Effect of SQUID's inductance on the noise

However, the maximizing of the flux-transfer factor alone does not necessarily yield the maximum in the S/N-ratio. The flux noise $\langle \Phi_n^2 \rangle^{1/2}$ is proportional to the self-inductance L of the SQUID. The proportionality depends on the structure and construction of the SQUID and has the form [Zim 71, Kur 73, Jac 75]

$$\langle \Phi_{ni}^2 \rangle^{1/2} \propto L^x, \quad 1/2 \leq x \leq 5/6 \quad (19)$$

The value of x must be determined for each SQUID system because it depends on which part dominates in the SQUID system's noise [Cla 75]. When the flux-transformer is coupled to the SQUID, its inductance changes. Then the effective self-inductance of the SQUID is

$$L_e = L - \frac{M_s^2}{L_s + L_d} = L[1 - k_s^2 L_s (L_s + L_d)^{-1}] \quad (20)$$

As can be seen, when the flux-transformer is coupled, the self-inductance of the SQUID decreases and thus the intrinsic flux-noise level is lower. In this case according to Eq. (14) the S/N-ratio is

$$\begin{aligned} \frac{S}{N} &= \frac{F \Delta \Phi_e}{\langle \Phi_{nc}^2 \rangle^{1/2}} \\ &= \frac{N_d M_s}{L_d + (1 - k_s^2) L_s} \cdot \frac{\Delta \Phi_e}{\langle \Phi_{nc}^2 \rangle^{1/2}} = \frac{N_d M_s}{L_d + (1 - k_s^2) L_s} \cdot \frac{\Delta \Phi_e}{\langle \Phi_{no}^2 \rangle^{1/2}} \cdot \left(\frac{L}{L_e} \right)^x \\ &= \frac{N_d k_s (L_s L)^{1/2}}{L_d + (1 - k_s^2) L_s} \cdot \frac{\Delta \Phi_e}{\langle \Phi_{no}^2 \rangle^{1/2}} \cdot \frac{1}{[1 - k_s^2 L_s / (L_s + L_d)]^x} = \frac{F_e \Delta \Phi_e}{\langle \Phi_{no}^2 \rangle^{1/2}}, \end{aligned} \quad (21)$$

where $\langle \Phi_{nc}^2 \rangle^{1/2}$ = the noise flux in the SQUID when the superconducting transformer circuit is connected,
 $\langle \Phi_{no}^2 \rangle^{1/2}$ = the noise flux in the SQUID when the signal coil is open,

F_e = the effective flux-transfer factor when the system noise is assumed to be independent of the detection coil coupling and equal to $\langle \Phi_{no}^2 \rangle^{1/2}$.

Lower limit of the interdependence of flux noise and SQUID self-inductance ($x=1/2$)

Next we will examine the two limiting cases of Eq. (19). It is first assumed that x has the value of $1/2$. Then maximizing Eq. (21) with respect to L_s gives:

$$L_s = \frac{L_d [k_s^2 + (k_s^4 - k_s^2 + 1)^{1/2}]}{1 - k_s^2} \quad (22)$$

According to Eq. (21) the effective flux-transfer factor is then

$$F_e = \frac{k_s (L_s L)^{1/2} N_d (L_d + L_s)^{1/2}}{[L_d + (1 - k_s^2) L_s]^{3/2}} \quad (23)$$

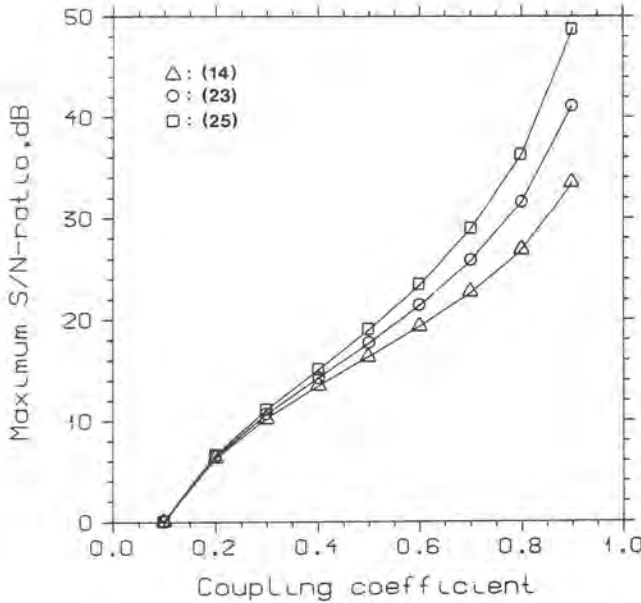


Figure 10. Maximum signal-to-noise ratios calculated by using Eqs. (23) and (25) as a function of the coupling coefficient k_s are compared to the S/N-ratio calculated with Eq. (14), where 0 dB level is set to the case when $k_s = 0.1$. In all cases L_d has the value calculated from Eqs. (22), (24) and (15), respectively.

Upper limit of the interdependence of flux noise and SQUID self-inductance ($x=1$)

The upper limit of the dependence of the flux noise exists when $x = 5/6$. However, this is quite close to the case when $x = 1$, which gives a good approximation. When maximizing Eq. (21) with respect to L_s when $x = 1$ we have in the maximum

$$L_s = \frac{L_d[3k_s^2 + 2(9k_s^2/4 - k_s^2 + 1)^{1/2}]}{2(1 - k_s^2)} \quad (24)$$

The effective flux-transfer factor in this case when $x = 1$ is given by

$$F_e = \frac{k_s(L_s L)^{1/2} N_d(L_d + L_s)}{[L_d + (1 - k_s^2)L_s]^2} \quad (25)$$

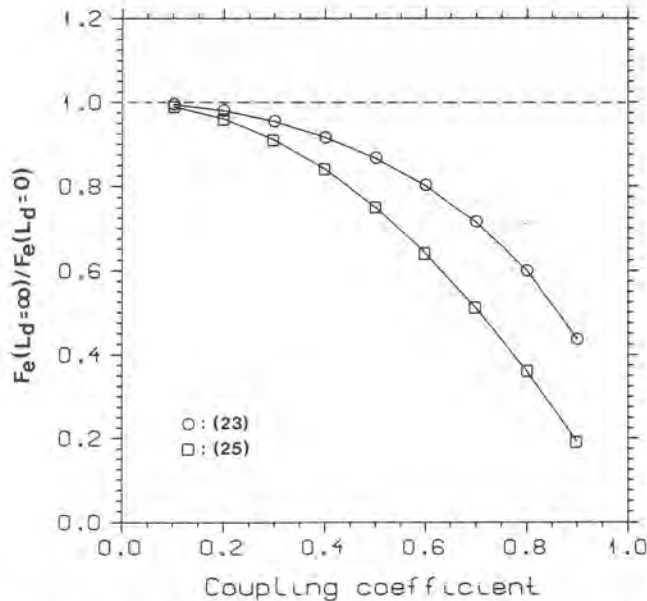


Figure 11. Ratio between the effective flux-transfer factors with two values, $L_d = \infty$ and $L_d = 0$, in both cases when $x = 1/2$ and $x = 1$ (Eqs. (23) and (25)) plotted as a function of the coupling coefficient k_s . When the difference in the noise between the cases $L_d = \infty$ and $L_d = 0$ is measured when the coupling coefficient is 0.3, the value is between 4.5% and 9% of the total noise depending on x .

The maximum signal-to-noise ratios (L_d has the optimum value) calculated by using Eqs. (23) and (25) are compared in Fig. 10 to the S/N-ratio calculated by using Eq. (14) as a function of the coupling coefficient k_s . The S/N-ratio calculated with Eq. (14) has been set to 0 dB when $k_s = 0.1$. The maximum increase of 15 dB in the S/N-ratio when compared to the S/N-ratio calculated with Eq. (14) is obtained when $k_s = 0.9$ and $x = 1$. The corresponding increase with k_s equal to 0.3 is only 0.8 dB. In Fig. 11 there is shown the ratio between the two flux-transfer factors when $L_d = \infty$ and $L_d = 0$ in both cases when $x = 1$ and $x = 1/2$. As can be seen, with small values of k_s it is difficult to determine the value of x from the noise measurements because the difference in noise between the cases $L_d = 0$ and $L_d = \infty$ (Eqs. (20) and (21)) is only a few per cent.

Fig. 12 shows the optimum value of L_s compared to L_d as a function of the coupling coefficient k_s in the three cases where the S/N-ratio is calculated by using Eqs. (14), (23) and (25). If the value of L_d calculated from Eq. (15) is used in the cases where SQUID's noise is taken into account (Eqs. (23) and (25)), the error in the S/N-ratio with the coupling coefficient of 0.3 is 0.42 dB. In our case we have assumed that the x value is equal to $1/2$, because in our system the dominant contribution to $(\Phi_{nr}^2)^{1/2}$ is provided by the RF-amplifier. The measurement of x gave only indefinite results.

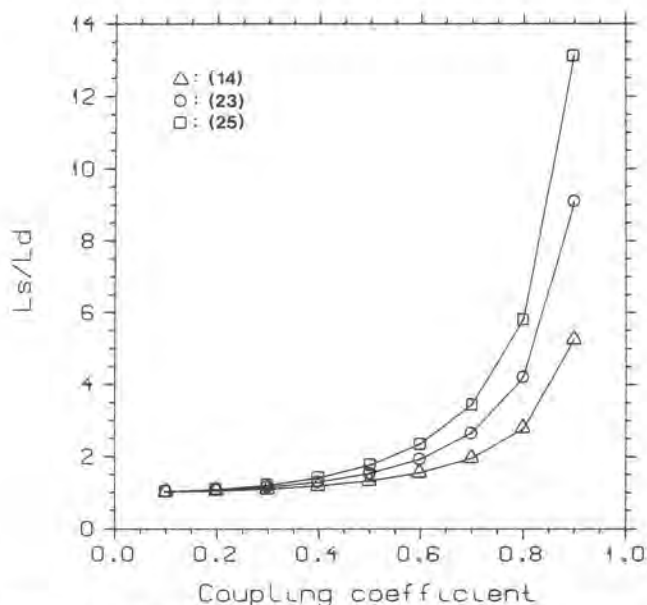


Figure 12. Optimum ratio of L_s/L_d as a function of the coupling coefficient k_s in three cases when the flux-transfer factor is calculated from Eqs. (14), (23) and (25).

5. OPTIMIZATION EQUATIONS

5.1. Source models

When the magnetic field of the heart is measured with the unipositional lead system, the source of the magnetic activity is modelled with a magnetic dipole in the center of the heart. However, although this theoretical point source describes acceptably the detected field patterns, the source of the magnetic field is still a distributed current inside the real heart muscle. To study the effect of a distributed current source on the optimization of the gradiometer, we have also tested other types of source models. In addition to the magnetic dipole, a current loop and a spherical current surface were examined in coaxial situation (X direction).

Current loop

The magnetic dipole moment \bar{m}_l of a current loop is

$$\bar{m}_l = I_l A_e \bar{n} \quad , \quad (26)$$

where I_l = the current of the loop,
 A_e = the effective area of the loop,
 \bar{n} = the unit vector normal to the loop.

When the distance to the loop is long when compared to its radius, the field of the loop is similar to the field of a magnetic dipole.

Current surface

The current surface model is a ball whose surface is covered with a homogeneous current distribution. This current is modelled with several loops lying on the ball's surface, each carrying the same current. The magnetic dipole moment \bar{m}_b of a spherical current surface modelled with N loops can be expressed approximately as

$$\bar{m}_b = I_l \left(\sum_{i=1}^N A_i \right) \bar{n} \quad , \quad (27)$$

where I_i = the current of the loops,
 A_i = the effective area of the i :th loop,
 \bar{n} = the unit vector directed towards the axis of the loops.

In all models used, magnetic dipole, current loop and spherical current surface, the equivalent magnetic dipole moment was set to $1 \mu\text{Am}^2$ when the optimization calculations were performed. The radius of the current loop and ball was set to 50 mm.

5.2. Signal-to-noise ratio

The optimization of the dimensions and structure of the gradiometers was made with respect to the signal-to-noise ratio. When a first-order gradiometer is used the S/N-ratio can be written as

$$\frac{S}{N} = \frac{\Phi_{sq}}{\langle \Phi_n^2 \rangle^{1/2}} = \frac{F_e \alpha \Delta \Phi_e}{\langle \Phi_n^2 \rangle^{1/2}} = \frac{k_s (L_s L)^{1/2} (L_g + L_s)^{1/2} \left(\frac{L_1}{L_g} \right)^{1/2} \Delta \Phi_g}{[L_g + (1 - k_s^2) L_s]^{3/2} \langle \Phi_n^2 \rangle^{1/2}}, \quad (28)$$

where Φ_{sq} = the magnetic flux in the SQUID caused by the signal,
 $\langle \Phi_n^2 \rangle^{1/2}$ = the equivalent magnetic flux noise of the system referred to the SQUID,
 F_e = the effective flux-transfer factor,
 α = the square root of the ratio of the pick-up coil inductance L_1 to the total inductance L_g of the gradiometer,
 $\Delta \Phi_e$ = the external magnetic flux difference between the pick-up and second coil, respectively,
 $\Delta \Phi_g$ = the magnetic flux of the gradiometer.

It must be noted that if the magnetic flux noise term $\langle \Phi_n^2 \rangle^{1/2}$ is expressed in $T_{rms}(Hz)^{-1/2}$, Eq. (28) gives the right result only when the S/N-ratio is calculated on a 1 hertz bandwidth. Otherwise the bandwidth of the measurement system and the spectrum distribution of the signal must be taken into consideration. In the following discussion the signal-to-noise ratio is expressed in dB on a 1 Hz bandwidth. The constant value of $8.5 \cdot 10^{-5} \Phi_o (Hz)^{-1/2}$ has been used for $\langle \Phi_n^2 \rangle^{1/2}$. In Eq. (28) the effect of SQUID's effective inductance on the noise is taken into consideration in F_e .

Magnetic dipole source

When the gradiometer is coaxial (in X direction) and has asymmetric construction with circular coils, and the source is a magnetic dipole \bar{m} on its axis, the gradiometer flux $\Delta\Phi_g$ can be written as (Fig. 3a)

$$\Delta\Phi_g = \frac{\mu_o m_x}{2} \left[\sum_{i=1}^{N_1} \frac{R_1^2}{(R_1^2 + h_i^2)^{3/2}} - \sum_{j=1}^{N_2} \frac{R_2^2}{(R_2^2 + h_j^2)^{3/2}} \right], \quad (29)$$

where m_x = the X component of the source dipole,
 R_1, R_2 = the radii of the pick-up and second coil, respectively,
 h_i, h_j = the distances from the source to the center of each loop of the pick-up and second coil, respectively.

When the gradiometer has a planar structure with circular coils (Y and Z gradiometers in Fig. 2) the magnetic flux of the gradiometer has to be calculated with integral equations. In the Y direction $\Delta\Phi_g$ has the form

$$\Delta\Phi_g = \frac{\mu_o m_y}{4\pi} \left\{ \sum_{i=1}^{N_1} \int_0^{2\pi} \int_0^{R_1} \frac{2D_i^2 - \rho_1^2}{(\rho_1^2 + D_i^2)^{5/2}} \delta d\delta d\alpha \right. \\ \left. - \sum_{j=1}^{N_2} \int_0^{2\pi} \int_0^{R_2} \frac{2D_j^2 - \rho_2^2}{(\rho_2^2 + D_j^2)^{5/2}} \delta d\delta d\alpha \right\}, \quad (30)$$

where m_y = the Y component of the source dipole,
 D_i, D_j = the distance from the center of the coil loop to the X axis for the pick-up coil and second coil, respectively,
 $\rho_1^2 = h^2 - 2h\delta \cos \alpha + \delta^2$,
 $\rho_2^2 = (h + b)^2 - 2(h + b)\delta \cos \alpha + \delta^2$.

The double integrals of Eq. (30) are computed numerically. The parameters of Eq. (30) are shown in Fig. 3c. In the case where there is a rectangular cross section in the Y coil, $\Delta\Phi_g$ becomes

$$\Delta\Phi_g = \frac{\mu_o m_y}{2\pi} \left\{ \sum_{i=1}^{N_1} \int_0^{C/2} \int_{-A/2}^{A/2} \frac{2D_i^2 - \rho_1^2}{(\rho_1^2 + D_i^2)^{5/2}} dx' dz' \right. \\ \left. - \sum_{j=1}^{N_2} \int_0^{C/2} \int_{-A/2}^{A/2} \frac{2D_j^2 - \rho_2^2}{(\rho_2^2 + D_j^2)^{5/2}} dx' dz' \right\}, \quad (31)$$

where $\rho_1^2 = (h + x')^2 + z'^2$,
 $\rho_2^2 = (h + b + x')^2 + z'^2$.

The parameters of Eq. (31) are shown in Fig. 4d.

Current loop source

When a current loop with radius R_l and current I_l is used as the source, the magnetic flux in the coaxially situated gradiometer is

$$\Delta\Phi_g = \mu_0 I_l \left\{ \sum_{i=1}^{N_1} [r_i^2 + (R_1 + R_l)^2]^{1/2} \left[\left(1 - \frac{k_i^2}{2}\right) K(k_i) - E(k_i) \right] - \sum_{j=1}^{N_2} [r_j^2 + (R_2 + R_l)^2]^{1/2} \left[\left(1 - \frac{k_j^2}{2}\right) K(k_j) - E(k_j) \right] \right\}, \quad (32)$$

where $k_i^2 = 4R_1 R_l [r_i + (R_1 + R_l)^2]^{-1}$,
 $k_j^2 = 4R_2 R_l [r_j + (R_2 + R_l)^2]^{-1}$,

and where functions K and E are complete elliptic integrals of the first and second kind, respectively. The parameters of Eq. (32) are shown in Fig. 13 for a single loop of a coil. The elliptic integrals are calculated by using their series approximations.

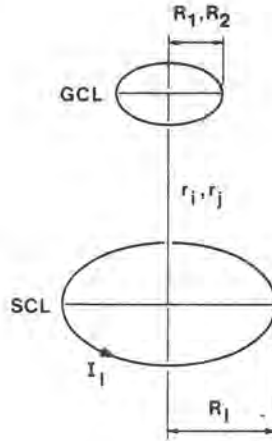


Figure 13. Geometry for calculating the magnetic flux through one loop of the gradiometer coil (GCL) generated by the current I_l in the source current loop (SCL).

5.3. Sensitivity

The sensitivity of the gradiometer is equal to that magnetic flux density \bar{B}_{min} in the pick-up coil which causes in the SQUID a magnetic flux equal to the equivalent magnetic flux noise of the system $\langle \Phi_n^2 \rangle^{1/2}$ referred to the SQUID or according to Eq. (28)

$$B_{min} = \frac{\langle \Phi_n^2 \rangle^{1/2}}{N_1 \pi R_1^2 F_c \alpha} \quad (33)$$

Here it is assumed that the magnetic field is coupled only to the pick-up coil and the field is homogeneous inside the coil. Thus Eq. (33) presents the maximum available sensitivity in theory when the baseline is very long but the second coil still loads the signal (α in Eq. (33)). The sensitivity of a gradiometer designed for maximum S/N-ratio is not necessarily equal to the maximum sensitivity for the given space limits.

6. RESULTS

The optimization was made by assuming that the coupling coefficient k_c was equal to 0.3. The baseline b of the gradiometer was set to 150 mm. The length of the gradiometer's coils was limited to 10 mm because in this case the effect of the coil length on the accuracy was not examined. Three different gradiometers were studied; a symmetric one where the ratio between the area of the second and pick-up coil, $\eta = A_2/A_1$, was equal to 1, and two asymmetric gradiometers where the ratios of the areas were $\eta = 2$ and $\eta = 3$.

6.1. X gradiometer

The X gradiometer was studied in three cases: when the distance from the source 1) to the center of its pick-up coil, 2) to the lower end of its pick-up coil and 3) to the periphery of the pick-up coil of the Y gradiometer (Fig. 2) was fixed.

The maximum available S/N-ratio in the X direction was first calculated by using Eqs. (28) and (29) for all three gradiometer structures as a function of the maximum coil radius in the case when the distance h_c from the source to the center of the pick-up coil was equal to 100 mm. The maximum radius of the X coil is the same as the radius R_{max} of the cryostat's inner space. As can be seen in Fig. 14, the change in the S/N-ratio with respect to the R_{max} is similar between the different three structures. The difference in the S/N-ratio is only about 1.5 dB maximum. The symmetric gradiometer with $\eta = 1$ shows the best S/N-ratio within the whole range. The S/N-ratio of the symmetric structure, however, seems to increase more slowly than that of the two others when R_{max} increases.

6.1.1. Effect of the pick-up coil length

In Fig. 15 there are shown the maximum S/N-values for the three gradiometer structures when the length of the pick-up coil is taken into consideration. This is the usual measurement situation when only the X

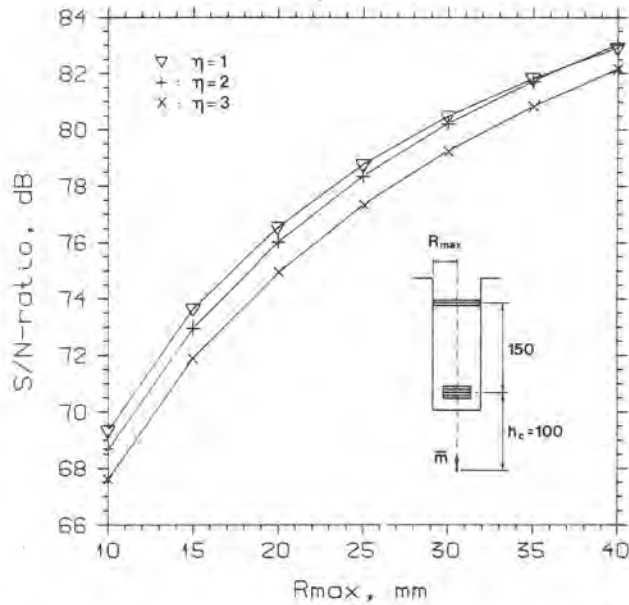


Figure 14. Maximum available signal-to-noise ratio for three different coaxial X gradiometers with circular coils as a function of the cryostat's inner radius. The distance h_c from the center of the pick-up coil to the magnetic dipole source \bar{m} is fixed to $h_c = 100$ mm. The magnetic dipole moment of the source was $1\mu Am^2$. The equivalent SQUID's flux noise and the coupling coefficient k_s to the SQUID were $8.5 \cdot 10^{-5} \Phi_o (Hz)^{-1/2}$ and 0.3, respectively.

component has to be recorded and the distance from the source to the inner bottom of the cryostat has a certain minimum (the shortest possible measurement distance). In this case the distance from the source to the lower end of the pick-up coil remains unchanged ($h_c = 100$ mm) and thus the total distance between the source and the center of the coil is $h_c + l_p/2$, where l_p is the length of the pick-up coil. It is very interesting to note that in this case also the symmetric structure shows the best S/N-ratio. It is over 1 dB better than the asymmetric gradiometer with $\eta = 2$ and nearly 3 dB better than that with $\eta = 3$. Thus for single component measurement, if the maximum S/N-ratio is desired, a symmetric gradiometer is recommended when the inner diameter of the cryostat is below 80 mm. The dimensions and data for the optimum gradiometer ($\eta = 1$) when the length of the pick-up coil is taken into consideration and when $R_{max} = 25$ mm are presented in Table 2. If a good spatial resolution of the measurement is considered, the situation is different.

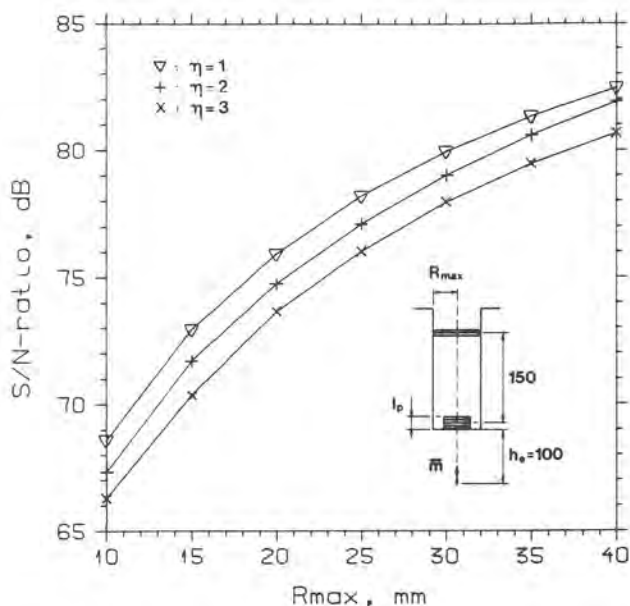


Figure 15. Maximum available S/N -ratio for three different coaxial x gradiometers with circular coils as a function of the cryostat's inner radius. The distance h_e from the pick-up coil's lower end to the source was fixed at $h_e = 100\text{mm}$.

Table 2. Dimensions and data of the X gradiometer for the optimum S/N -ratio when $h_e = 100\text{ mm}$

	Pick-up coil	Second coil
Radius, mm	25.00	25.00
Length, mm	2.0	10.0
Number of turns	9	9

Baseline = 150 mm , Inductance = 16.8 μH
 S/N -ratio = 78.2 dB , Sensitivity = 20.3 $fT_{rms}(Hz)^{-1/2}$

The sensitivity of each three types of gradiometers was examined by using Eq. (33). When the S/N-ratio is at an optimum, the corresponding sensitivity is shown in Fig. 16 as a function of R_{max} for the three structures. As can be seen, the change of the sensitivity is similar for each type.

The effect of the coupling coefficient and measurement distance on the optimum signal-to-noise ratio was examined when R_{max} was equal to 25 mm. In Fig. 17 the optimum S/N-ratio is presented as a function of the coupling coefficient k_s . The difference between the S/N-ratios of the three structures remains the same. This same effect was noted also when the S/N-ratio was calculated as a function of the measurement distance with k_s equal to 0.3.

All the calculations above were made when the length of the coils was limited to 10 mm. In Fig. 18 there is shown the effect of the coil length on the S/N-ratio calculated with Eqs. (28) and (29) for one symmetric and two asymmetric ($\eta = 2$ and $\eta = 3$) gradiometers, respectively. The number of turns of both gradiometer coils was fixed in each case to the values obtained from optimization with the maximum 10 mm coil length in each case. Fig. 18 shows that the S/N-ratio increases when the length l_s of the second coil increases. For the symmetric gradiometer the S/N-ratio increases when the length l_p of the pick-up coil decreases. However, when the second coil is long, the effect of the pick-up coil length on the S/N-ratio is smaller. The best result is obtained when the pick-up coil is wound a few millimetres long and the second coil is made as long as possible. For the asymmetric gradiometers the situation is different. For the structure with $\eta = 2$ the optimum length of the pick-up coil increases from 3 mm to 9 mm when the length of the second coil increases from 1 mm to 20 mm. For the asymmetric gradiometer with $\eta = 3$ the optimum length of the pick-up coil is 8 mm when l_s is 1 mm, and it increases to 16 mm when l_s is 20 mm.

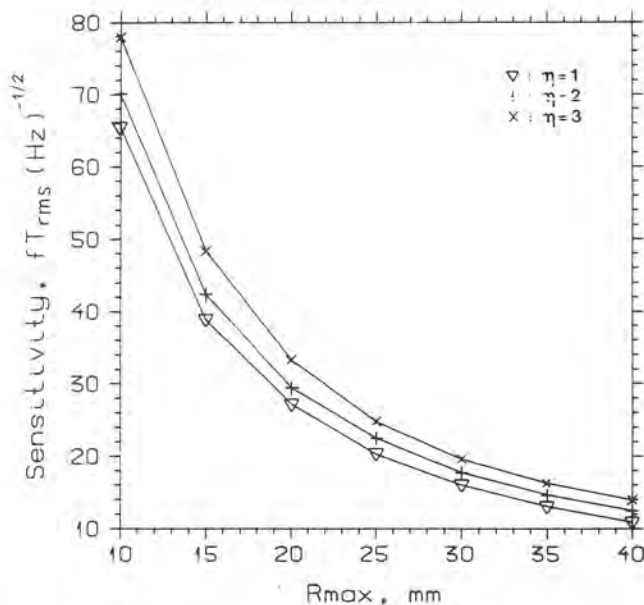


Figure 16. Sensitivity of the three different optimum coaxial X gradiometers of Fig. 15 when optimized with respect to the S/N-ratio.

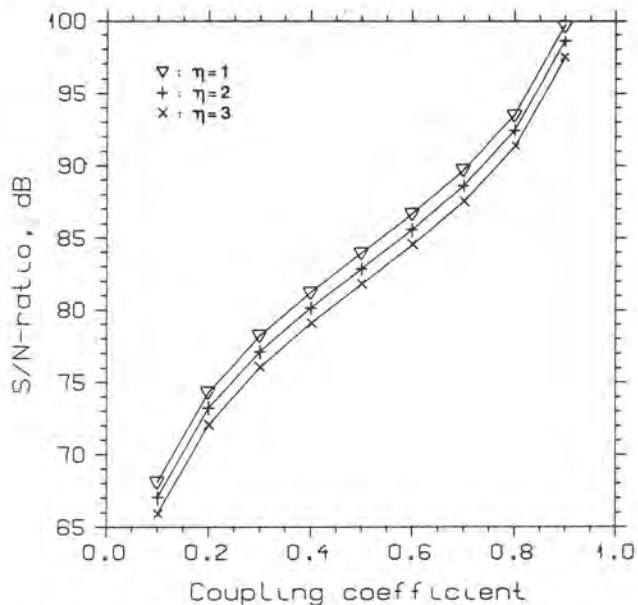


Figure 17. Maximum S/N-ratio of three different coaxial X gradiometers with circular coils as a function of the coupling coefficient k_e . The inner radius of the cryostat was 25 mm and the distance h_e was fixed at 100 mm.

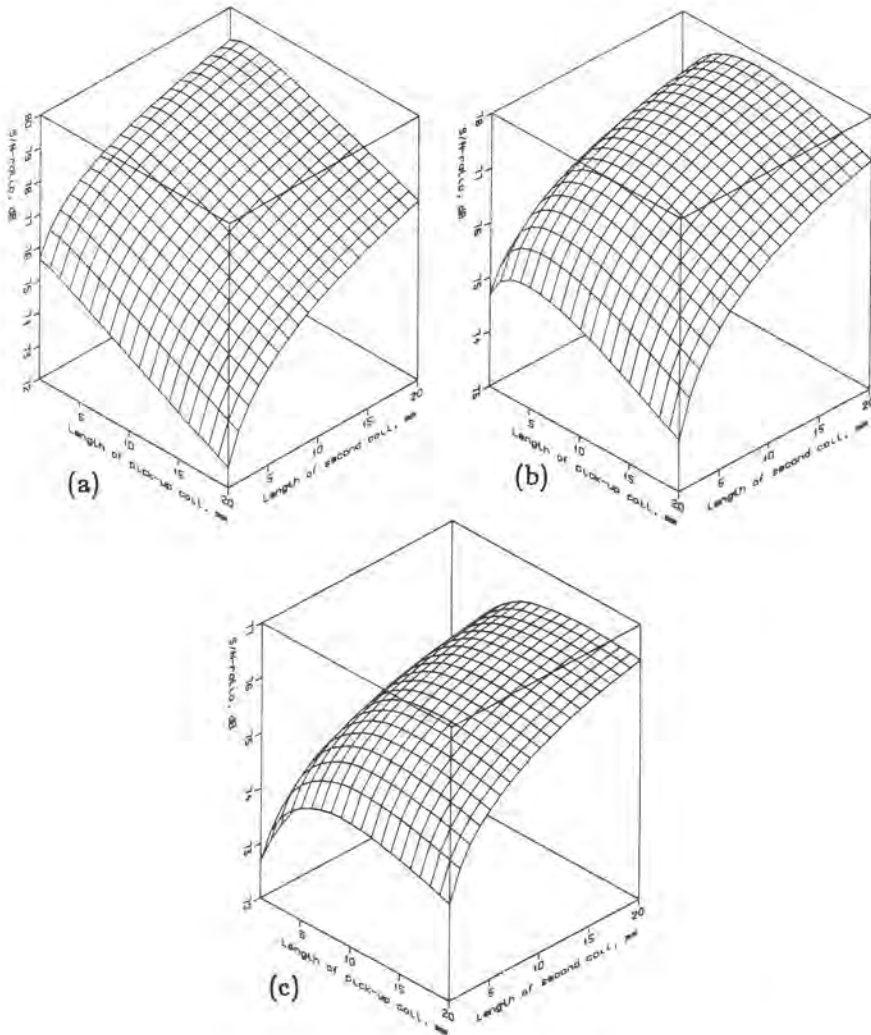


Figure 18. Effect of the length of the pick-up and second coil to the S/N-ratio in three cases; (a) the gradiometer is symmetric or $\eta = 1$; (b) asymmetric, $\eta = 2$; (c) asymmetric, $\eta = 3$. The numbers of turns of the gradiometer coils are fixed in each case at the values obtained from optimization with maximum 10 mm coil length.

6.1.2. Effect of the Y coil radius

Fig. 19 shows the calculated maximum available S/N-ratio for the X gradiometer with circular coils when it is assumed to be a part of a vector gradiometer as presented in Fig. 2. In this structure the Y and Z coils are similar to the X coil. Now the distance between the source and the center of the pick-up coil is $h_p + R_{1y}$, where R_{1y} is the radius of the pick-up coil in the Y gradiometer (or Z gradiometer) and the distance h_p between the source and periphery of the Y coil is fixed and equal to 100 mm. In this case the worst signal-to-noise ratio is obtained with the symmetric gradiometer when $R_{max} > 18$ mm. The asymmetric gradiometer with $\eta = 2$ has the maximum S/N-ratio over the whole examined range. On the

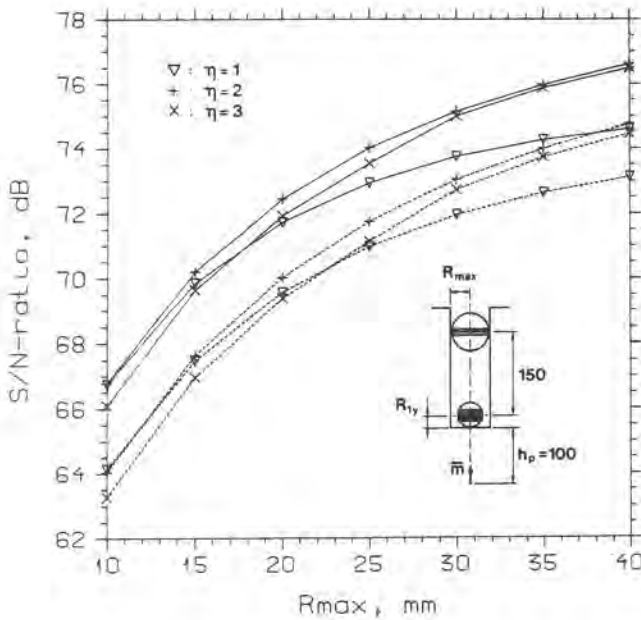


Figure 19. Maximum S/N-ratio for X gradiometers with circular coils as a function of the cryostat's inner radius. The distance h_p from the periphery of the pick-up coil of the Y gradiometer (Fig. 2) to the source is fixed at $h_p = 100$ mm. The calculations are made with two sources: the solid lines are obtained in the case when a magnetic dipole source was used, and the dashed lines when the source was a current loop with a radius of 50 mm. In both cases the magnetic dipole moment of the source was $1 \mu Am^2$.

Table 3. Dimensions and data of the X gradiometer for the optimum S/N-ratio when $h_p = 100$ mm

	Pick-up coil	Second coil
Radius, mm	17.67	25.00
Length, mm	10.0	10.0
Number of turns	16	8

Baseline = 150 mm , Inductance = 17.2 μH
 S/N-ratio = 74.0 dB , Sensitivity = 21.7 $fT_{rms}(Hz)^{-1/2}$

small values of the radius it is about 0.6 dB better than the gradiometer with $\eta = 3$, and 2 dB better than the symmetric case when ($R_{max} = 40$ mm). The dimensions and data for the optimum gradiometer structure when $R_{max} = 25$ mm are presented in Table 3. The sensitivity in this case when the S/N-ratio is at a maximum is equal to the maximum available sensitivity.

6.1.3. Effect of the source type

The results presented above were obtained with a magnetic dipole as source. The effect of the current loop source and spherical current surface source on the results was also studied by using Eq. (32).

A current loop with the radius of 50 mm and the equivalent dipole moment of $1\mu Am^2$ as the source gives similar results as the magnetic dipole. The only difference in the optimized structure of the gradiometer when compared to the structure obtained with a dipole source can be found in asymmetric gradiometers where the length of the pick-up coil tends to increase by the order of ten per cent for the optimum result. In

Fig. 19 there are shown also the calculated optimum S/N-ratios of three different X gradiometers when the source is a current loop at the distance of 100 mm from the periphery of the Y pick-up coil. The form of the curves when compared to the case with a dipole source is similar, although the obtained S/N-ratios with the current loop source are lower.

The spherical current surface source with the radius of 50 mm, the number of loops of 41 and the equivalent dipole moment the same as with the loop source gives in all cases equivalent results with the dipole source. The effect of the source type was examined only in the coaxial situation.

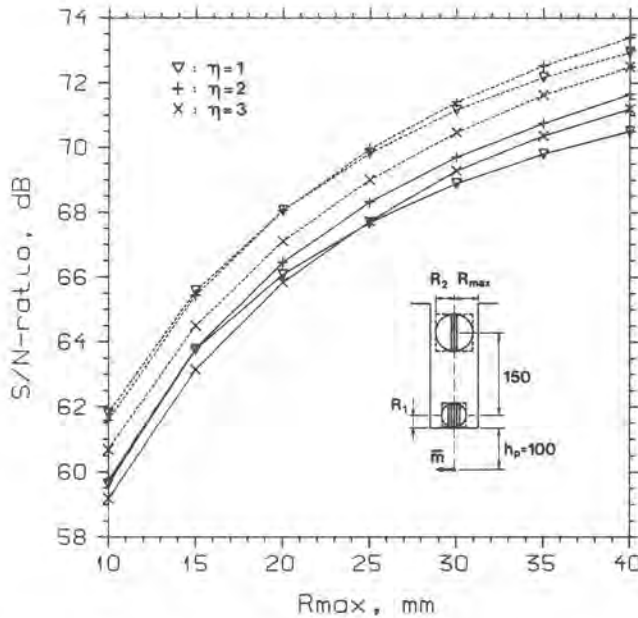


Figure 20. Maximum S/N-ratio for planar Y gradiometers as a function of the cryostat's inner radius when the cross-section of the gradiometer coils is circular (solid lines) and rectangular (dashed lines). The distance h_p from the periphery of the pick-up coil to the source is fixed at 100 mm. In gradiometers with rectangular coils the coil area is equal to the area of a circular coil with radius $R = C/2$. In asymmetric gradiometers the pick-up coil's height is lower whereas the width remains the same.

6.2. Y and Z gradiometer

The Y gradiometers were studied only in the case where the distance h_p from the source to the periphery of the pick-up coil was fixed. Thus the distance to the center of the pick-up coil is $h_p + R_1$. The results with Z gradiometers are equivalent with those of Y gradiometers.

6.2.1. Circular coils

The optimum S/N-ratio for three different planar Y gradiometers with circular coils is shown in Fig. 20 as a function of R_{max} . The maximum length of the coils is set to 10 mm. As can be seen in this case the asymmetric gradiometer with $\eta = 2$ shows the best S/N-ratio. It is about 0.7 dB above the value obtained with both other structures when $R_{max} = 25$ mm. Both asymmetric structures have quite similar optimum S/N-curves. The symmetric gradiometer has the worst S/N-ratio when $R_{max} > 24$ mm. The dimensions and data of the optimum gradiometer structure when $R_{max} = 25$ mm are presented in Table 4. The coil dimensions of the planar gradiometers differ from the dimensions of the X coils because in

Table 4. Dimensions and data of the Y gradiometer for the optimum S/N-ratio when $h_p = 100$ mm

	Pick-up coil	Second coil
Radius, <i>mm</i>	17.30	24.47
Length, <i>mm</i>	10.0	10.0
Number of turns	16	8

Baseline = 150 *mm*, Inductance = 16.7 μH
 S/N-ratio = 68.3 *dB*, Sensitivity = 22.3 $f T_{rms}(Hz)^{-1/2}$

this case the maximum radius R_2 of the second coil is not the same as the radius R_{max} of the inner space of the cryostat. Because the length l_2 of the second coil must now be taken into account, it follows that $R_{max} = [R_2^2 + (l_2/2)^2]^{1/2}$ and optimum values for both the radius and the length of the second coil can be found.

6.2.2. Rectangular coils

The properties of the rectangular Y coil were first tested with a single loop on the X axis by using a magnetic dipole source in the origin. The magnetic flux was calculated through the rectangular loop whose maximum width was limited by the inner diameter of the cryostat ($R_{max} = 25$ mm) and whose area was set equal to the area of a circular loop with radius R_{max} (equal sensitivity with X loop). In Fig. 21 there is shown the relative change of the magnetic flux through such a loop as a function of the width of the loop in two cases. The upper curve is obtained when the distance ($h_c = 120$ mm) is from the source to the center of the loop. In this case the flux increases when the height of the loop increases while the area remains constant. In the lower curve the distance ($h_p = 100$ mm) to the periphery of the loop remains constant and thus the distance to the center is $100 \text{ mm} + A/2$, where A is the height of the loop. The lower curve describes the situation in a vector gradiometer where the distance from the cryostat's bottom is determined by the height of the Y and Z pick-up coil. According to these results, the width C of the pick-up coil in asymmetric planar Y and Z gradiometers with rectangular coils should be equal to $2[R_{max}^2 - (l_p/2)^2]^{1/2}$ for the maximum S/N-ratio.

The only question concerning a planar gradiometer with rectangular coil cross section is thus the optimum ratio of the coil length to the coil width. In Fig. 20 there are shown the optimized S/N-ratios for the symmetric and two asymmetric ($\eta = 2, \eta = 3$) structures as a function of R_{max} . In the symmetric structure the ratio between the width and height of both coils is $C/A = 4/\pi$ (the area of the rectangular coil is equal to the area of a circular coil with radius $C/2$). In asymmetric cases with $\eta = 2$ and $\eta = 3$ the ratios are $C/A = 8/\pi$ and $C/A = 12/\pi$, respectively. The best S/N-ratio is obtained with the asymmetric structure with $\eta = 2$ when $R_{max} > 20$ mm, whereas below that radius the symmetric structure is slightly better. The optimum result with a rectangular coil when compared to the planar structure with circular coils is 2 dB higher when R_{max} is 25 mm.

6.3. Optimum construction of vector gradiometer

In Table 5 there are shown dimensions and data of a vector gradiometer optimized for our measurements. The asymmetric structure where $\eta = 2$ has been used. The gradiometer coils are similar in both

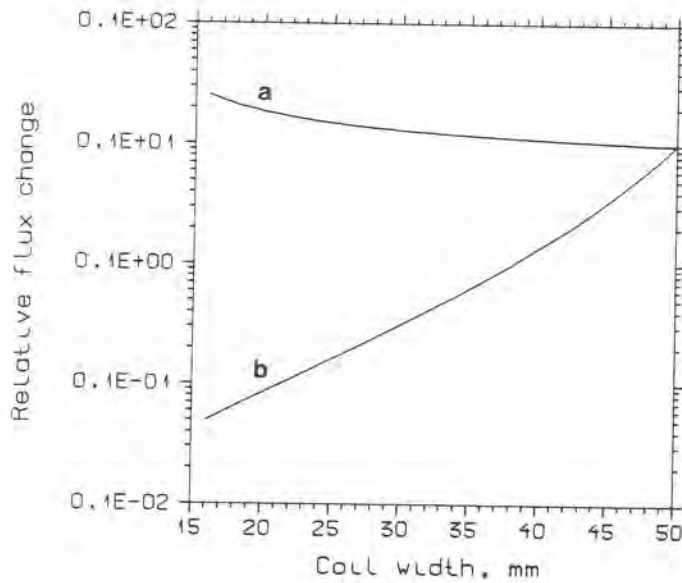


Figure 21. Relative change in the calculated magnetic flux through a rectangular Y loop as a function of the loop's width in two cases; (a) the distance from the loop's center to the source (magnetic dipole) is fixed (120 mm); (b) the distance from the loop's periphery to the source is fixed (100 mm). In both cases the flux is set to 1 when the coil width is 50 mm. The area of the loop is maintained the same during calculations (= the area of a circular coil with a radius of $C/2$; Fig. 4).

coaxial and planar structures. Circular cross-section has been chosen for all coils. In the pick-up coil of the X gradiometer the length/radius-ratio is 1.8 which allows the measuring of a magnetic dipole as close as 40 mm from the center of the coil with the maximum error of 2% in accuracy (Fig. 3a). In the Y and Z pick-up coils the length/radius-ratio is 1.36. With this ratio the magnetic dipole source can be as close as 30 mm from the center of the coil with a maximum error of 2%.

In Fig. 22 is shown an example of a magnetic heart vector recorded in the magnetically shielded room of Tampere University of Technology. The measurement is made from a healthy 28-year-old male in real time with a multiplexed vector magnetometer [Lek 84] by using the corrected unipositional lead system [Esk 84]. The noise level is of the order of $100 f T_{rms}(Hz)^{-1/2}$.

Table 5. Dimensions and data of a vector gradiometer for the optimum S/N-ratio when $h_p = 100$ mm

	Pick-up coil	Second coil
X gradiometer:		
Radius, <i>mm</i>	16.20	22.91
Length, <i>mm</i>	29.0	20.0
Number of turns	22	11
Y and Z gradiometer:		
Radius, <i>mm</i>	16.20	22.91
Length, <i>mm</i>	22.0	20.0
Number of turns	22	11

Baseline = 150 *mm*

Sensitivity; X: $20.3 f T_{rms}(Hz)^{-1/2}$ Y,Z: $20.5 f T_{rms}(Hz)^{-1/2}$

S/N-ratio; X: 75.2 *dB* Y,Z: 69.2 *dB*

Inductance; X: 17.7 μH , Y,Z: 19.9 μH

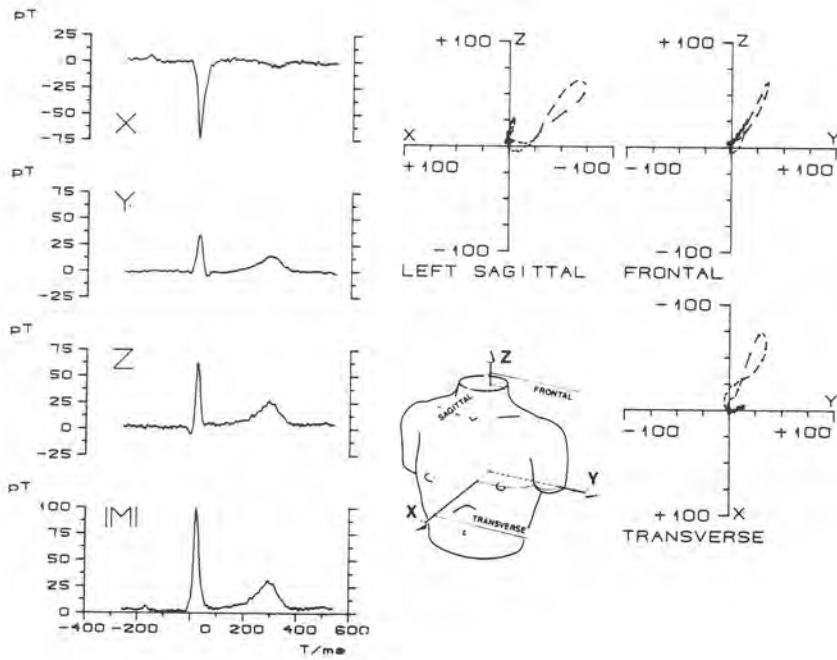


Figure 22. Real time recording of the magnetic heart vector from a 28-year-old male. The measurement is performed with a multiplexed vector magnetometer using the unipositional lead system. The measurement distance is 106 mm.

7. DISCUSSION

In the theoretical measurement situation where the source of the magnetic field is modelled by a magnetic dipole, the dimensions of the pick-up coil have a clear influence on the accuracy of the determination of the source dipole. In this study we have designed the vector gradiometer so that if the location of the source is known it is possible to determine the magnitude of a magnetic dipole anywhere in the heart muscle region from the measured coil flux.

In a real heart the source is the distributed current density. This current density can be modelled by elementary current dipoles distributed in the myocardium. The ideal lead field of a magnetic lead has zero sensitivity to all current dipoles on the symmetry axis and linearly increasing tangential sensitivity as a function of a radial distance from the symmetry axis. Thus only the vortex sources will generate the magnetic field. However, a problem arises because the sum of all those magnetic sources is measured and the equivalent magnetic dipole is assumed to be in the center of the heart. Only those sources which are located at an appropriate distance from the detector have the correct effect on the output when compared to the ideal lead field (Eq. (1)). The proximity effect distorts the result by increasing the effect of proximal sources and by attenuating distal sources.

A very interesting question is whether it is possible by using an appropriate coil design to partially compensate for the proximity effect. If we look at Figs. 3 and 4, where the effect of the coil length on the accuracy is shown, it seems that when the X coil is very short its response to the proximal sources is less than it should be when calculated according to the dipole theory. Correspondingly, when Y coil is long, the same effect can be seen. Especially in the case of a rectangular coil with the ratio $C/A = 3$ (Fig. 4c) the effect is apparent over a wide range. However, this is true only of the magnetic dipole sources. When we have a current dipole source in a homogeneous volume conductor the situation is different because the electric currents in the conducting media are not necessarily magnetically dipolar.

We have tested the effect of the coil dimensions on the measurement accuracy by using the same geometry as Wikswo [Wik 78] where the coil is on the positive x-axis and the source is a current dipole \vec{p}_y which is located in a conducting half-space at point $(-X_d, 0, Z_d)$ (Fig. 23). The

air-conductor interface is the YZ plane. The coil flux can be written in this case by using complete elliptic integrals $K(k)$ and $E(k)$ as [Wik 78]

$$\Phi_d = \frac{\mu_0 p_y}{\pi} \sum_{i=1}^{N_d} \frac{\sqrt{R/Z_d}}{k_i} \left[\left(1 - \frac{k_i^2}{2}\right) K(k_i) - E(k_i) \right], \quad (34)$$

where $k_i^2 = 4Z_d R [(Z_d + R)^2 + (h_i + X_d)^2]^{-1}$.

Correspondingly, the X component of the magnetic field density B_{cdip} in the center of the coil caused by the current dipole \bar{p}_y is [Wik 78]

$$B_{cdip} = \frac{\mu_0 p_y}{4\pi} \frac{Z_d}{[Z_d^2 + (h + X_d)^2]^{3/2}}. \quad (35)$$

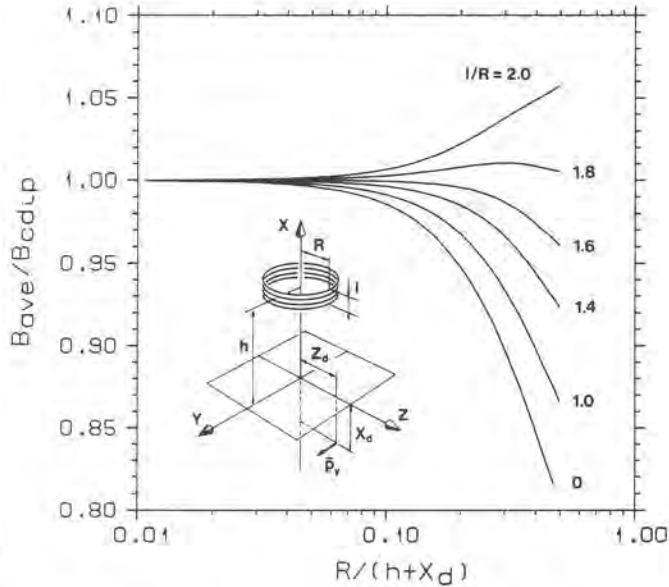


Figure 23. Ratio between the magnetic flux density B_{ave} , calculated from the coil flux, and the flux density B_{cdip} , calculated from the dipole equation, in the center of the coil with different ratios of l/R . The coil is circular and its turn density is l/R . The source is a current dipole \bar{p}_y located in the conducting half-space at the point $(-X_d, 0, Z_d)$ and directed along the Y axis. The air-conductor interface is the YZ plane.

Fig. 23 shows the ratio between the flux density B_{ave} calculated from the coil flux, Eq. (34), and the flux density B_{cdip} calculated from Eq. (35) as a function of the ratio between the coil radius and the coil's vertical distance from the source for different length/radius-ratios. Here Z_d and X_d are set equal to R . As can be seen, the situation is similar to that with a magnetic dipole source (Fig. 3a). Better measurement accuracy is obtained if the current dipole source is deeper in the conducting half-space or if the dipole's distance from the X axis is longer. According to Fig. 23, the design of the coil dimensions is important when examining electric dipolar sources which are in the vicinity of the coil, as for example in magnetoencephalography.

8. SUMMARY

The vector gradiometer structure which shows the best sensitivity and minimum error when determining a magnetic source dipole was investigated. The optimization of the structure was made with respect to the S/N-ratio when the space for the gradiometer in the cryostat was limited and the distance between the source and the inner bottom of the cryostat was fixed.

The effect of the gradiometer's dimensions on the accuracy of the determination of the source was examined. It was found that with coaxial circular coils the best length/radius-ratio is about 1.7 ($\sqrt{3}$) when the turn density is high. With circular Y coils the optimum ratio is of the order of 1.5, i.e. smaller than that obtained with the Taylor series expansion. With these lengths it is possible to measure the strength of a magnetic dipole at a distance as short as $2R$, where R is the coil radius, with a maximum error of 3%. When the turn density of the coil is lower, the optimum length/radius-ratio decreases. For the X coil with two loops the optimum ratio is 1 i.e. the loops are separated by R , whereas for the Y coil the ratio is 0.9. Using rectangular Y coils it is not possible to obtain the accuracy of circular coils with as short measurement distances, on the contrary, the corresponding distances are 10 - 20 times longer. The baseline of the vector gradiometer was determined with reference to the physical dimensions of the source and the measurement distance.

The coupling of the detection coil to the SQUID and the effect of the flux-transfer factor on the S/N-ratio were studied. It was found that the dependence of the SQUID's noise level on its own self-inductance is an important fact when the coupling coefficient k_s between the SQUID's signal coil and SQUID ring is high. The so called effective flux-transfer factor was derived in the two limiting cases when the SQUID's noise is proportional to $L^{1/2}$ and L , where L is the self-inductance of the SQUID. Calculation of the optimum detection coil inductance was studied in both cases and compared to the normal case, when it is determined from $L_d = L_s(1 - k_s^2)$, where L_s is the signal coil inductance. The equations for optimization calculations are presented.

The signal source was modelled with a magnetic dipole, but also current loop and spherical current surface source models were used. The source type was found to have only a minor effect on the optimal dimen-

sions. In all cases, three different basic structures were optimized, one symmetric and two asymmetric gradiometers where the ratio η between the areas of the second and pick-up coil was 2 and 3, respectively. The optimum S/N-ratio was determined by calculating the signal flux in the SQUID with all gradiometer structures and taking the maximum of these.

The optimization was made for the X gradiometer with circular coils in three cases when the distances from the source to 1) the center of the pick-up coil, 2) the lower end of the pick-up coil and 3) the periphery of the pick-up coil in the Y direction were fixed. In Y and Z gradiometers the optimization was made with both circular and rectangular coils when the distance from the source to the periphery of their pick-up coil was fixed.

If only one component (X component) is measured and the distance from the cryostat to the source is fixed, the highest signal is obtained with the symmetric gradiometer when the maximum coil radius R_{max} is below 40 mm. With all gradiometer types the S/N-ratio increases when the length of the second coil increases. In the symmetric case the length of the pick-up coil should be short, whereas for both asymmetric cases an optimum length can be found. In the vector gradiometer the optimum dimensions of the X gradiometer depends on the structure of Y and Z gradiometers. With circular Y and Z coils the X gradiometer with $\eta = 2$ has the maximum S/N-ratio. It is 2 dB better than the symmetric one when $R_{max} = 40$ mm. When the Y and Z coils are rectangular, the S/N-ratios of different structures of the X gradiometer are the same as in Fig. 14 because the distance no longer depends on the X coil radius. In Y and Z gradiometers with circular coils both aforementioned asymmetric gradiometers are better than the symmetric one when $R_{max} > 25$ mm. However, when $R_{max} < 15$ mm the symmetric structure shows the best S/N-ratio. With rectangular coils the worst S/N-ratio is obtained with the asymmetric gradiometer where $\eta = 3$, whereas both other structures have similar S/N-ratio curves. For rectangular coils the S/N-ratios are over 2 dB higher than with circular coils.

REFERENCES

- [Bau 70] Baule, G. and McFee, R., The magnetic heart vector. *Am. Heart J.* **79**(1970)2, p. 223-236.
- [Bru 83] Bruno, A.C. and Costa Ribeiro, P., A symmetric third order gradiometer without external balancing for magnetocardiography. *Cryogenics* **23**(1983)6, p. 324-326.
- [Cla 75] Claassen, J.H., Coupling considerations for SQUID devices. *J. Appl. Phys.* **46**(1975)5, p. 2268-2275.
- [Coh 70] Cohen, D., Edelsack, E.A. and Zimmerman, J.E., Magneto-cardiograms taken inside a shielded room with a superconducting point-contact magnetometer. *Appl. Phys. Lett.* **16**(1970)7, p. 278-280.
- [Coh 82] Cohen, D., Steady fields of the body. *Biomagnetism, Proceedings of a NATO Advanced Study Institute on Biomagnetism*. New York and London, Plenum Press, 1982, p. 327-340.
- [Dur 83] Duret, D. and Karp, P., Instrumentation for biomagnetism. *Il Nuovo Cimento, Proceedings of the Fourth International Workshop on Biomagnetism* **2D**(1983)2, p. 123-141.
- [Ehn 75] Ehnholm, G.J., Soini, J.K. and Wiik, T., Thin film SQUIDs using superconducting tunnel junctions. *Proceedings of the Fourteenth Intern. Conf. on Low Temp. Phys.* . Otaniemi, Finland, Aug 14-20, **4**(1975), p. 234-237.
- [Esk 83] Eskola, H. and Malmivuo, J., Optimizing vector magnetocardiographic lead fields by using a physical torso model. *Il Nuovo Cimento, Proceedings of the Fourth International Workshop on Biomagnetism* **2**(1983)2, p. 356-367.
- [Esk 84] Eskola, H.J., Malmivuo, J.A.V., Nousiainen, J.J.O. and Lekkala, J.O., Corrected unipositional lead system for vector magnetocardiography. *IEEE Trans. Biomed. Eng.* (to be published).
- [Gro 46] Grover, F.W., *Inductance calculations* . New York, D. Van Nostrand Company, 1946.

- [Jac 75] Jackel, L.D. and Burhmann, R.A., Noise in the rf SQUID. *J. Low Temp. Phys.* **19**(1975)3/4, p. 201-246.
- [Kar 80] Karp, P. and Duret, D., Unidirectional magnetic gradiometers. *J. Appl. Phys.* **51**(1980)3, p. 1267-1272.
- [Kur 73] Kurkijärvi, J., Noise in the superconducting quantum flux detector. *J. Appl. Phys.* **44**(1973)8, p. 3729-3733.
- [Lan 67] Langford-Smith, F., *Radio designers handbook*. London, Iliffe Books Ltd., 1967.
- [Lek 82] Lekkala, J. and Malmivuo, J., SQUID vectormagnetometer for biomagnetic instrumentation. *Proceedings of the World Congress on Medical Physics and Biomedical Engineering 1982*. Hamburg, Jürgen Kinzel, 1982, p. 2.04
- [Lek 84] Lekkala, J. and Malmivuo, J., SQUID vectormagnetometer for biomagnetic instrumentation. *J. Phys. E: Sci. Instrum.* **17**(1984), (in press).
- [Lou 74] Lounasmaa, O.V., *Experimental principles and methods below 1K*. London, Academic Press, 1974.
- [Mal 76] Malmivuo, J., On the detection of the magnetic heart vector - An application of the reciprocity theorem. *Acta Polytechnica Scandinavica EL 39*, Thesis, Helsinki 1976.
- [Ode 78] Odehnal, M., Petříček, R., Tichy, R. and Tomášek, F., Low-level SQUID magnetometry of the human heart in a small ferromagnetic enclosure. *Cryogenics* **18**(1978)7, p. 427-431.
- [Rom 82] Romani, G.L., Williamson, S.J. and Kaufman, L., Biomagnetic instrumentation. *Rev. Sci. Instrum.* **53**(1982)12, p. 1815-1845.
- [Sep 83] Seppänen, M., Katila, T., Tuomisto, T., Varpula, T., Duret, D. and Karp, P., Measurement of biomagnetic fields using multi-channel superconducting-magnetometer techniques. *Il Nuovo Cimento, Proceedings of the Fourth International Workshop on Biomagnetism* **2D**(1983)2, p. 166-174.
- [Sto 83] Storey, J.R., Magnetic sensors with good signal-to-interference discrimination. *Il Nuovo Cimento, Proceedings of the Fourth International Workshop on Biomagnetism* **2D**(1983)2, p. 153-165.

- [Var 82] Varpula, T., Karp, P., Katila, T., Poutanen, T. and Seppänen, M., A three-channel superconducting vector magnetometer. *Proc. XVI Annual Conference of the Finnish Physical Society*. Espoo, Finland, (1982)Feb, p. 8:23.
- [Vrb 82] Vrba, J., Fife, A.A. and Burbank, M.B., Spatial discrimination in SQUID gradiometers and 3rd order gradiometer performance. *Can. J. Phys.* **60**(1982)1, p. 1-12.
- [Wik 75] Wikswo, J.P. *Non-invasive Magnetic Measurement of the Electrical and Mechanical Activity of the Heart*. Thesis. Stanford University, Stanford 1975.
- [Wik 78] Wikswo, J.P., Jr., Optimization of SQUID differential magnetometers. *AIP Conference Proc.* **44**, New York, American Institute of Physics, 1978.
- [Wil 81] Williamson, S.J. and Kaufman, L., Biomagnetism. *Journal of Magnetism and Magnetic Materials* **22**(1981), p. 129-201.
- [Zim 71] Zimmerman, J.E. and Frederick, N.V., Miniature ultra-sensitive magnetic gradiometer and its use in cardiography and other applications. *Appl. Phys. Lett.* **19**(1971)1, p. 16-19.
- [Zim 77] Zimmerman, J.E., SQUID instruments and shielding for low-level magnetic measurements. *J. Appl. Phys.* **48**(1977)2, p. 702-710.